SCIENCE CHINA
Information Sciences

• RESEARCH PAPER •

August 2026, Vol. 69, Iss. 8, 182206:1–182206:22
https://doi.org/10.1007/s11432-024-4888-8

Relations of PE level for RBF neural networks under the discrete-time framework and their application to deterministic learning

Weiming WU†, Jinyuan ZHANG†, Chen SUN, Qinghua SUN, Juanjuan XU & Cong WANG*

School of Control Science and Engineering, Shandong University, Jinan 250061, China

Received 26 March 2024/Revised 20 January 2025/Accepted 25 August 2025/Published online 31 July 2026

Abstract The persistent excitation (PE) condition is one of the most important concepts for various adaptive algorithms. At present, more efforts have been made to study the PE condition for sufficiency. However, there are fewer studies on the excitation level, which commonly acts as a constant of convergence relation, affecting the performance of the algorithm. This paper establishes the PE level relations for radial basis function (RBF) neural networks under the discrete-time framework. From the standpoint of network parameters, the PE level is proportional to the separation distance and tends to diminish as the excitation distance grows larger. Furthermore, the PE level reaches its optimal value when the receptive field width is appropriately chosen. From the perspective of discrete signal properties, the PE level is observed to increase as the sampling period decreases or as the trajectory velocity slows down. As an illustration, based on the relations of PE level, the performance of deterministic learning under the sampled data framework is established for analysis. The results show that the existence of an optimal separation distance leads to maximum learning accuracy, caused by the trade-off between the approximation ability of the neural network and the excitation level. Moreover, the existence of an ill-conditioned interpolation matrix related to the interpolation method also yields the optimal receptive field width. A simulation example is used to demonstrate the effectiveness of the PE level relations obtained.

Keywords persistent excitation condition, adaptive algorithm, deterministic learning, persistent excitation level, radial basis function neural networks

Citation Wu W M, Zhang J Y, Sun C, et al. Relations of PE level for RBF neural networks under the discrete-time framework and their application to deterministic learning. Sci China Inf Sci, 2026, 69(8): 182206, https://doi.org/10.1007/s11432-024-4888-8

1 Introduction

Persistent excitation (PE) is an essential concept related to parameter learning in adaptive control and identification [1, 2]. As a necessary and sufficient condition for accurate parameter identification [3–5], PE ensures that the parameter estimation proceeds with asymptotic/exponential convergence to true values [6, 7]. For linear systems, PE is related to the "sufficient richness" of the input frequencies [4, 8]. However, for nonlinear systems, the PE condition is hard or sometimes impossible to verify *a priori* [9], since the additional frequencies derived from the nonlinear transformations might cancel out and impede PE [10]. Especially for the neural identification problem, no guarantee of true convergence of weights without the satisfaction of the PE condition will inevitably cast doubts on the power of the neural identification approach [9].

Fortunately, in recent years, it has been found that the regression vectors possess the potential to satisfy the PE condition through radial basis function (RBF) mapping [11–14]. To this end, radial basis function neural networks (RBFNNs) have been widely popular as universal approximators [15] in adaptive control and identification fields [16–19]. In [11], it is shown that the regressor vector satisfies the PE condition when the input to an RBFNN coincides with all its neuron centers. Such an assumption is relaxed by [12], only requiring the inputs to belong to a certain neighborhood of the neuron centers constructed on a regular lattice. Further, Ref. [13] proposed the PE condition for the regressor vector consisting of neuron centers that are periodically visited by the inputs in a

* Corresponding author (email: wangcong@sdu.edu.cn)
† These authors contributed equally to this work.

neighborhood with no more than the neuron separation distance. Recently, Refs. [14, 20] extended the neighborhood size of [13] and derive a sufficient condition for PE for any recurrent trajectory.

Based on the recent progress of PE condition for RBFNNs, a mechanism called deterministic learning is developed for locally accurate learning/modeling of inherent system dynamics [14, 20]. The true value convergence of RBFNN weights is guaranteed by the exponential stability of a class of adaptive linear time-varying (LTV) systems under the PE condition. Owing to the ability of accurate dynamics modeling, deterministic learning can be well applied to many tasks in dynamic environments. For the control tasks, the accurate modeling of closed-loop system dynamics can be reused in similar control tasks to enhance control performance [21, 22]. For the recognition tasks, the acquired inherent dynamics can be used for effectively representing and distinguishing dynamical patterns [23, 24]. Recent studies [25, 26] have found that a low PE level may result in deterioration of the performance of modeling of deterministic learning, leading to poor performance in the aforementioned downstream tasks. Besides, the PE level is also crucial in the quantitative performance analysis of adaptive algorithms [13, 25–29]. Therefore, it is of both theoretical and practical importance to explore the strategy for improving the PE level.

For the sufficiency of the PE condition, many new breakthroughs have been made more recently. A sufficient condition of PE defined over embedded manifolds in the reproducing kernel Hilbert spaces is derived in [29]. In [30], the persistent excitation condition for the signal transformed by means of polynomials is proposed. For single hidden-layer neural networks using step or ReLU activation functions, Ref. [31] established the sufficient condition for PE. Moreover, the PE condition for deep neural networks has been explored in [32, 33]. However, there are few results providing quantitative analysis of PE level improvement. For linear time-invariant (LTI) systems, PE can be quantified as the minimum singular value of an input Hankel matrix [34]; yet the PE condition is algorithm-dependent for nonlinear systems [9].

In this paper, based on our previous result [35], the relations between the RBFNN's structure parameters and the PE level are established under the discrete-time framework. From the standpoint of network parameters, the PE level is linearly proportional to the separation distance between neurons, decreases as the excitation distance increases, and reaches an optimal value when the receptive field width is appropriately chosen. From the perspective of discrete signal properties, the PE level is linearly and inversely proportional to the sampling period and increases as the trajectory velocity slows down. Furthermore, the performance analysis of deterministic learning under the sampled-data framework is taken to illustrate the application of the obtained results in the convergence analysis of identification algorithms based on RBF networks. Regarding the RBFNN's structure parameters, an optimal separation distance between neurons exists that maximizes learning accuracy, resulting from a trade-off phenomenon between the PE level and the approximation ability of the RBFNN. Meanwhile, due to a severely ill-conditioned interpolation matrix caused by a large receptive field width and a low-dimensional approximation space related to a small receptive field width, there also exists an optimal receptive field width of neurons to achieve the highest learning accuracy. The proposed results are verified in the numerical simulation section. In summary, the explicit relations for the PE level of RBFNN under a discrete-time framework are given and applied to analyze the performance of deterministic learning. Our contribution can be summarized as follows.

- Inspired by the work in [36], by relaxing the excitation distance condition of its Proposition 3.12, explicit relations of PE level for the RBFNN are established, which are more concise and compact compared with the relations derived by [35].
- Relations of PE level for the RBFNN under the continuous time framework [35] are developed to the discrete-time framework. The direct relationships are established with some properties of the discrete-time system, such as the sampling period and the system trajectory velocity, leading to theoretical guidance for the performance analysis of discrete-time algorithms (e.g., adaptive control, identification, and learning) based on RBFNN.
- Based on the derived relations, the performance analysis of deterministic learning, as reported in [25, 26, 37], can be further extended to using the RBFNN's structure parameters, lending another perspective of theoretical guidance for the performance optimization of deterministic learning algorithms in engineering applications.

2 Preliminaries

Notation. $\mathbb{R}$ and $\mathbb{N}^*$ denote, respectively, the set of real numbers and the set of natural numbers without zero; $\mathbb{R}_+$ denotes the set of positive real numbers; $\mathbb{R}^{m\times n}$ and $\mathbb{R}^n$ denote, respectively, the set of $m \times n$ real matrices and the set of $n \times 1$ real column vectors (or n-dimensional Euclidean space); for any $x \in \mathbb{R}^n$, $\|x\|$ denotes its Euclidean norm and x^{T} denotes its transpose; $|\cdot|$ denotes the absolute value of a real number. The definitions of some variables in this paper are given in Table 1.

Table 1 Definition of variables.

Variable	Definition
Z	Input trajectory
$Z[k]$	Sampling points of trajectory Z
h	Separation distance of RBF network
ε	Excitation distance of RBF network
η	Receptive field width of the neuron of RBF network
κ	Trajectory velocity
T_s	Sampling period
μ	PE level

2.1 Radial basis function neural networks

2.1.1 *Global approximation property*

For a continuous function $f(x) : \Omega \to \mathbb{R}$, RBFNNs are applied to approximate as

$$f(Z[k]) = W^{*\mathrm{T}} S(Z[k]) + \epsilon(Z[k]), \quad \forall Z[k] \in \Omega, \tag{1}$$

where $\Omega \subset \mathbb{R}^m$ is a compact set, $Z[k]$ denotes the input discrete signal of NN (also called the sampling point), $W^* \in \mathbb{R}^N$ is the ideal weight vector and N is the number of neuron centers, $S(Z[k]) = [s_1(Z[k]), s_2(Z[k]), \ldots, s_N(Z[k])]^{\mathrm{T}} \in \mathbb{R}^N$ denotes the regressor vector consisting of the radial basis function $s_i(Z[k])$. Consider here $s_i(Z[k])$ as the Gaussian function $\exp\left(\left(-(Z[k]-\xi_i)^{\mathrm{T}}(Z[k]-\xi_i)\right)/\eta_i^2\right)$, where ξ_i denotes neuron arranged in the input space and η_i denotes the receptive field width of the neuron ξ_i. For the Gaussian RBFNN, there exists $\|S(\cdot)\| \leqslant S_m \in \mathbb{R}_+$ [13]. $\epsilon(Z[k])$ denotes the discrete-time approximation error with $|\epsilon(Z[k])| \leqslant \epsilon^*$ is satisfied, where $\epsilon^* \in \mathbb{R}_+$ is small enough.

2.1.2 *Localized approximation property*

For any input trajectory Z with sampling points $Z[k]$, $f(Z[k])$ can be approximated by a finite number of excited neurons along the trajectory in a localized region, yielding the following local approximation:

$$f(Z[k]) = W_\zeta^{*\mathrm{T}} S_\zeta(Z[k]) + \epsilon_\zeta(Z[k]), \quad \forall Z[k] \in \Omega, \tag{2}$$

where the subscript $(\cdot)_\zeta$ denotes the neurons excited by the region closed to the input trajectory, $W_\zeta^* \in \mathbb{R}^{N_\zeta}$, $S_\zeta(Z[k]) = [s_{1\zeta}(Z[k]), \ldots, s_{j\zeta}(Z[k])]^{\mathrm{T}} \in \mathbb{R}^{N_\zeta}$ denotes the localized regressor vector consisting of the excited neurons, with $N_\zeta < N$, and $\epsilon_\zeta(Z[k])$ is the localized discrete-time approximation error with $\epsilon_\zeta = O(\epsilon)$ is satisfied.

The following definitions of RBFNN's structure parameters are introduced.

Definition 1 (Separation distance [38]). For RBFNN, the separation distance h between neurons is given by

$$h := \frac{1}{2} \min_{j \neq k} \|\xi_j - \xi_k\|, \quad \forall \xi_j, \xi_k \in \Xi, \tag{3}$$

where $\Xi := \{\xi_j\}_{j=1}^N \subset \Omega$ denotes the set of neurons.

For a sampling point set $X := \{X[k]\}_{k=1}^M \subset \Omega$, the separation distance h_X between sampling points is given by

$$h_X := \frac{1}{2} \min_{i \neq j} \|X[i] - X[j]\|, \quad \forall X[i], X[j] \in X. \tag{4}$$

Definition 2 (Fill distance [38]). For RBFNN, the fill distance $h_{\Xi,\Omega}$ is given by

$$h_{\Xi,\Omega} := \sup_{x \in \Omega} \min_{\xi_j \in \Xi} \|x - \xi_j\|. \tag{5}$$

For a sampling point set $X := \{X[k]\}_{k=1}^M \subset \Omega$, the fill distance $h_{X,\Omega}$ is given by

$$h_{X,\Omega} := \sup_{x \in \Omega} \min_{X[k] \in X} \|x - X[k]\|. \tag{6}$$

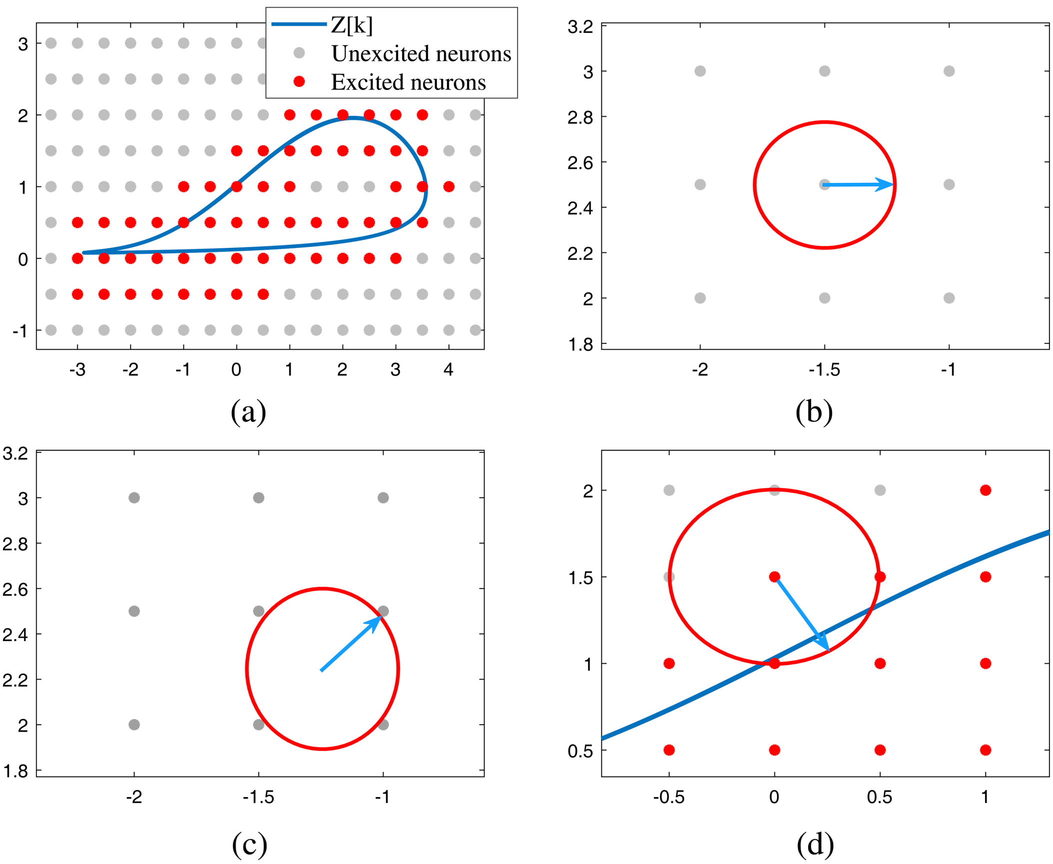

Figure 1 (Color online) An example for demonstration. (a) Excited neurons and trajectory; (b) separation distance; (c) fill distance; (d) excitation distance.

Definition 3 (Excitation distance). For an input trajectory $Z \subset \Omega$, set $\varepsilon \in (0, \varepsilon']$, where $\varepsilon' > h$ is a positive constant, and let the localized regressor vector $S_\zeta(Z[k])$ be composed of the neurons ξ_j of the RBFNN that satisfy

$$\inf_{Z[k]\in Z} \|Z[k] - \xi_j\| \leqslant \varepsilon, \quad \forall \xi_j \in \Xi_\varepsilon, \tag{7}$$

where $\Xi_\varepsilon := \{\xi_j\}_{j=1}^{N_\zeta} \subset \Omega$ denotes the set of excited neurons. Then ε is defined as the excitation distance.

In Figure 1(b), the separation distance h is denoted geometrically as the radius of the largest possible empty ball drawn around each neuron center such that no ball intersects other balls; the fill distance $h_{\Xi,\Omega}$ (see Figure 1(c)) represents the radius of the largest possible empty ball that can be placed among the neuron centers inside Ω. The geometric interpretations of h_X and $h_{X,\Omega}$ are also similar to h and $h_{\Xi,\Omega}$. The excitation distance ε (see Figure 1(d)) is the neighborhood boundary of the corresponding neuron center when the scalar resulting from the nonlinear mapping via the radial basis function reaches a specific threshold value. Additionally, we let $k_\varepsilon = \varepsilon/h$, $k_{\varepsilon'} = \varepsilon'/h$, $k_\eta = \eta/h$ to simplify the presentation.

Due to the close relationship between the approximation ability of RBFNN and its structure parameters, we introduce here the lemma of discrete-time approximation error estimation based on Sobolev space for radial basis functions, which is presented in Proposition 3.3 of [38].

Lemma 1 (Approximation error [38]). Suppose $\tau = k + s$, where $k \in \mathbb{N}^*$ and $0 < s \leqslant 1$. Let α be a multi-index satisfying $k > |\alpha| + \frac{n}{2}$. Also, for a compact region $\Omega \subset \mathbb{R}^n$, let $\Xi := \{\xi_j\}_{j=1}^{N} \subset \Omega$ be a discrete set with fill distance $h_{\Xi,\Omega}$. Let $X := \{X[k]\}_{k=1}^{M} \subset \Omega$ be a second discrete set, with $h_{X,\Omega} \leqslant h_{\Xi,\Omega}$. If $f \in W_2^\tau(\Omega)$, and if $1 \leqslant q \leqslant \infty$, then

$$|f - I_\Xi f|_{w_q^{|\alpha|}(X)} \leqslant c \left(\frac{h_{X,\Omega}}{h_X}\right)^{\frac{n}{q}} h_{\Xi,\Omega}^{\tau-|\alpha|-n\left(\frac{1}{2}-\frac{1}{q}\right)_+} \|f\|_{W_2^\tau(\Omega)}, \tag{8}$$

where c is a constant independent of f and $h_{\Xi,\Omega}$, $(x)_+ = x$ if $x \geqslant 0$ and is 0 otherwise.

Remark 1. Herein, $I_{\Xi}f$ denotes the value of the interpolant. $W_p^{\tau}(\Omega)$ is a Sobolev space consisting of all functions $f:\Omega\to R$ such that $\partial^i f\in L_p$ for all weak partial derivatives of order $0\leqslant |i|\leqslant \tau$. $\|f\|_{W_p^{\tau}(\Omega)}$ refers to the Sobolev semi-norm. And $\ell_p(X)$-derivative norms are defined as follows:

$$|f|_{w_p^k(X)}=\begin{cases}\left(\sum\limits_{|\alpha|=k}\|\partial^\alpha f\|_{\ell_p(X)}^p\right)^{\frac{1}{p}}, & 1\leqslant p<\infty,\\ \sup\limits_{|\alpha|=k}\|\partial^\alpha f\|_{\ell_\infty(X)}, & p=\infty.\end{cases}\tag{9}$$

For a continuous function f defined on Ω,

$$\|f\|_{\ell_p(X)}=\begin{cases}\left(\dfrac{1}{M}\sum\limits_{k=1}^{M}|f(X[k])|^p\right)^{\frac{1}{p}}, & 1\leqslant p<\infty,\\ \max\limits_{1\leqslant k\leqslant M}|f(X[k])|, & p=\infty.\end{cases}\tag{10}$$

It can be seen that the approximation error increases with $h_{X,\Omega}/h_X$ and $h_{\Xi,\Omega}$ when the approximated function f is specific.

2.2 Persistent excitation

Definition 4 (Persistent excitation [39])**.** For the discrete-time case, if a vector-valued time series $S(Z[k]):\Omega\to\mathbb{R}^N$ is uniformly bounded and there exist positive constants μ, K and k' such that

$$\sum_{k=k'}^{k'+K-1}S(Z[k])\,S^{\mathrm{T}}(Z[k])\geqslant\mu I,\tag{11}$$

then $S(Z[k])$ is said to be PE and μ is the lower bound of persistent excitation, defined as the PE level.

Lemma 2 (PE condition [20])**.** For any periodic or recurrent trajectory $Z(t)\in\mathbb{R}^n\subset\Omega$ with Ω is a compact set, if the neuron centers of an RBF network are uniformly arranged and filled in the set Ω, and the size of the neuron neighborhood is extended to generate a subvector $S_\zeta(Z(t))$ consisting of the radial basis functions of all neurons close to the trajectory $Z(t)$, then the subvector $S_\zeta(Z(t))$ almost always satisfies the PE condition.

Moreover, for $Z_i\in\mathbb{R}^n$, $i=1,\ldots,N_\zeta$, define an interpolation matrix

$$A_\zeta=A_\zeta\left(Z_1,\ldots,Z_{N_\zeta}\right)=\begin{bmatrix}s\left(\|Z_1-\xi_1\|\right) & \ldots & s\left(\left\|Z_1-\xi_{N_\zeta}\right\|\right)\\ \vdots & \ddots & \vdots\\ s\left(\left\|Z_{N_\zeta}-\xi_1\right\|\right) & \ldots & s\left(\left\|Z_{N_\zeta}-\xi_{N_\zeta}\right\|\right)\end{bmatrix},\tag{12}$$

where $s(\cdot)$ is a radial basis function, then, for all constant-valued vectors $c\in\mathbb{R}^{N_\zeta}$ and a dense subset of the set Z_i that satisfy $\|Z_i-\xi_i\|\leqslant\varepsilon$, $i=1,\ldots,N_\zeta$ with $\sqrt{n}h\leqslant\varepsilon\leqslant\varepsilon'$ (i.e., $\sqrt{n}\leqslant k_\varepsilon\leqslant k_{\varepsilon'}$), there exist $\theta>0$ such that the following inequality holds

$$\|A_\zeta c\|\geqslant\theta\|c\|,\tag{13}$$

which means that A_ζ is nonsingular for a dense subset of Z_i.

The above lemma illustrates that the subvector $S_\zeta(Z(t))$ corresponding to the recurrent trajectory $Z(t)$ satisfies the PE condition under the continuous time framework, and in this paper, we will show that the subvector $S_\zeta(Z[k])$ still satisfies the PE condition under the discrete-time framework and give the relations of PE level.

2.3 Euler discretization of nonlinear system and system trajectory

In this paper, a general nonlinear system is considered as follows:

$$\dot{x}=F(x;p_s),\quad x(t_0)=x_0,\tag{14}$$

where $x=[x_1,\ldots,x_n]^{\mathrm{T}}\in\Omega$ denotes the state vector and $\Omega\subset\mathbb{R}^n$ is a compact set, p_s is the constant vector of system parameters. $F(x;p_s)=[f_1(x;p_s),\ldots,f_n(x;p_s)]^{\mathrm{T}}$ is a vector function consisting of unknown nonlinear smoothing functions with $\|F(x;p_s)\|\leqslant\kappa\in\mathbb{R}_+$.

Definition 5 (Recurrence [40])**.** For any constant $\nu > 0$, there exists a time coefficient $R_\nu > 0$ such that the trajectory $x(t)$ returns to its ν-neighborhood after time R_ν, then $x(t)$ is called the recurrent trajectory.

Assumption 1 (Recurrent trajectory)**.** The trajectories of the nonlinear system (14) are uniform-bounded, i.e., $x(t) \in \Omega$, $\forall t \geqslant t_0$, $x_0 \in \Omega$, where $\Omega \subset \mathbb{R}^n$ is a compact set. Additionally, the system trajectory starting from the initial state x_0 is recurrent.

The Euler discretization of system (14) is introduced as

$$x[k+1] = x[k] + T_s F(x[k]; p_s), \quad \forall k \geqslant 0, \tag{15}$$

where $x[k] = x(t_0 + kT_s)$ is the discrete-time state vector, and $T_s > 0$ is the sampling period.

Specifically, $Z = [Z[0], \ldots, Z[k]]^{\mathrm{T}} \subset \Omega$ is used to denote the input trajectory of neural network consisting of the input trajectory vector $Z[k] = [x_1[k], \ldots, x_n[k]]^{\mathrm{T}}$, where $x_i[k]$ is the state vector generated by the discrete-time nonlinear system (15). Under Assumption 1, the input trajectory Z here is the recurrent trajectory.

Recurrent trajectory includes a large class of trajectories generated from nonlinear dynamical systems, such as periodic, quasi-periodic, almost-periodic, and some chaotic trajectories [40].

2.4 Deterministic learning under sampled-data framework

The deterministic learning algorithm provides an effective method for dynamics modeling under sampled data generated by general nonlinear systems. It includes 4 elements [14, 20]: (i) RBFNN is applied; (ii) the PE condition for the RBF regressor vector along the recurrent trajectory is satisfied; (iii) a class of LTV systems satisfies exponential stability; (iv) locally-accurate modeling of the system dynamics is achieved along system trajectories. The following introduction of the deterministic learning algorithm is provided briefly.

According to (15), consider the dynamical RBFNN-based identifiers as follows:

$$\hat{x}_i[k+1] = \hat{x}_i[k] + (\alpha_i - 1)(\hat{x}_i[k] - x_i[k]) + \hat{W}_{\zeta i}^{\mathrm{T}}[k] S_\zeta(x[k]), \tag{16}$$

where $\hat{x}_i \in \mathbb{R}$ denotes the estimate state of the identifier, $0 < \alpha_i < 1$ is the identifier gain, $\hat{W}_{\zeta i} \in \mathbb{R}^{N_\zeta}$ denotes the estimated NN weight, $S_\zeta(x[k]) \in \mathbb{R}^{N_\zeta}$ is the RBF regressor vector and $\hat{W}_{\zeta i}^{\mathrm{T}}[k] S_\zeta(x[k])$ is the RBFNN for approximating the unknown nonlinear system dynamics $f_i(x[k]; p_s)$ of (15).

The RBFNN weights are updated by the learning law based on the Lyapunov stability is considered as follows:

$$\hat{W}_{\zeta i}[k+1] = \hat{W}_{\zeta i}[k] - T_s \gamma S_\zeta(x[k])(\hat{x}_i[k+1] - x_i[k+1]), \tag{17}$$

where $0 < \gamma < \frac{1}{2T_S^2 S_m^2}$ denotes the learning gain.

Combining (16) and (17) yields the deterministic learning error system

$$\begin{bmatrix} e_i[k+1] \\ \tilde{W}_{\zeta i}[k+1] \end{bmatrix} = \begin{bmatrix} \alpha_i & T_s S_\zeta^{\mathrm{T}}[k] \\ -\alpha_i T_s \gamma S_\zeta[k] & I - \gamma T_s^2 S_\zeta[k] S_\zeta^{\mathrm{T}}[k] \end{bmatrix} \begin{bmatrix} e_i[k] \\ \tilde{W}_{\zeta i}[k] \end{bmatrix} + \begin{bmatrix} -T_s \epsilon_{\zeta i}[k] \\ T_s^2 \gamma S_\zeta[k] \epsilon_{\zeta i}[k] \end{bmatrix}, \tag{18}$$

where $e_i = \hat{x}_i - x_i$ denotes the state tracking error, $\tilde{W}_{\zeta i} = \hat{W}_{\zeta i} - W_{\zeta i}^*$ denotes the estimation error of weight parameters and $|\epsilon_{\zeta i}[k]| < \bar{\epsilon}_{\zeta i} \in \mathbb{R}_+$ denotes the discrete-time approximation error of localized RBFNN. $S_\zeta[k]$, $\epsilon_{\zeta i}[k]$ are the simplification of $S_\zeta(x[k])$, $\epsilon_{\zeta i}(x[k])$, respectively.

From Theorem 2 in [26], the convergence relation of the system (18) is introduced by the following lemma.

Lemma 3 (Convergence relation [26])**.** Consider the learning error system (18) with the dynamical identifiers (16) and the weight update law (17). Under Assumption 1, if $0 < \alpha_i \leqslant \omega_i$ and $\frac{1}{\alpha_i} \leqslant \gamma \leqslant \frac{1}{2T_S^2 S_m^2}$ hold, the system (18) satisfies the following solution:

$$\|\chi_i[k]\| \leqslant \sqrt{c'} \sigma^k \|\chi_i[0]\| + b, \tag{19}$$

with

$$\sigma = \left(\omega_i^2 + \alpha_i^2 \gamma^2 T_s^2 S_m^2 + \alpha_i \gamma T_s S_m\right)^{\frac{1}{2}}, \tag{20}$$

$$b = \frac{T_s \sqrt{1 + \frac{\gamma}{2}} \bar{\epsilon}_{\zeta i}}{(1 - \sigma)\sqrt{1 - \omega_i^2}}, \tag{21}$$

where $\chi_i[k] = \left[e_i^{\mathrm{T}}[k], \tilde{W}_{\zeta i}^{\mathrm{T}}[k]\right]^{\mathrm{T}}$, $c' = \frac{1}{1 - \omega_i^2}$, and $\omega_i = \left(1 - \frac{2KT_s^2 \mu \gamma (2 - S_m^2 T_s^2 \gamma)}{(K-1)KS_m^4 T_s^4 \gamma^2 + 2(KS_m^2 - 1)T_s^2 \gamma + 2}\right)^{\frac{1}{2K}}$.

Under Assumption 1, the recurrent trajectory ensures that the RBF regression vector $S_\zeta\left(x\left[k\right]\right)$ satisfies the sufficiency condition for PE, with the regression vector consisting of the excited neurons along the trajectory [14]. In our recent result [26], based on the PE condition, the LTV system (18) has been given explicit relations for exponential convergence. It shows that the estimation error of weight parameters $\tilde{W}_{\zeta i}$ converges to a small neighborhood close to the origin, and the estimated NN weight $\hat{W}_{\zeta i}$ converges to its ideal weight $W^*_{\zeta i}$. Hence, the locally accurate modeling of the unknown system dynamics $f_i(x\left[k\right]; p_s)$ is achieved via the localized RBFNN.

3 Problem formulation

Recall the definition of PE and consider the subvector $S_\zeta\left(Z\left[k\right]\right)$ consisting of the neurons close to the input trajectory $Z\left[k\right]$:

$$\sum_{k=k'}^{k'+K-1} S_\zeta\left(Z\left[k\right]\right) S_\zeta^{\mathrm{T}}\left(Z\left[k\right]\right) \geqslant \mu I, \tag{22}$$

where μ is defined as the PE level.

Remark 2. Recently, there have been some developments in the study of sufficient conditions for PE, which are stated in detail in our introduction. However, only satisfying the sufficient condition for PE may not be sufficient to improve the performance of the algorithm. In most adaptive NN algorithms for control, identification, learning, and so on, the improvement of algorithmic performance often requires a higher PE level. In [13], it is shown that a high PE level enhances parameter convergence speed and accuracy, while in [25, 26], a low PE level deteriorates the modeling effectiveness of deterministic learning. Moreover, increasing the PE level may also improve the convergence performance of feedback feedforward neural network learning control [19], achieving high precision in adaptive feedforward neural network control [41], and enhancing the convergence speed and accuracy of the algorithm for adaptive neural identification and control of pure-feedback nonlinear systems [42]. Thus, the establishment of explicit relations for the PE level contributes to the study and improvement of algorithm performance.

However, there are few results providing quantitative analysis of PE level improvement. For nonlinear systems, the PE condition is algorithm-dependent [9]. The question of what kind of network satisfies the PE condition under what conditions is inherently a challenging problem. By extending the neighborhood size of [13], Refs. [14, 20] proved the PE condition for any recurrent trajectory. The PE level is directly related to the minimum eigenvalue of an interpolation matrix in Lemma 3.3 of [13]. By analyzing the minimum eigenvalue of the interpolation matrix, Ref. [35] gave the PE level relations for RBF networks under the continuous time framework.

Currently, the study of the PE level relations for RBF networks under the discrete-time framework remains an unexplored area. For practical applications, most algorithms need to be implemented within a discrete-time framework, and the signals generated by digital systems are intrinsically discrete sequences. Hence, some additional considerations, such as the choice of sampling period and discretization methods, can affect the performance and stability of the algorithms. Furthermore, the PE level of RBF networks is related to the trajectory of the nonlinear system. The trajectories of the sampled systems generated by employing different sampling periods and discretization methods for the same system are distinct, resulting in different PE levels. Therefore, based on the above discussion, establishing the relations of PE level for discrete-time systems is a challenging and important task.

Specifically, we describe the objective of this paper in two parts.

- Establish the relations of PE level from the perspective of both network structures and trajectory properties under the discrete-time framework.
- Analyze the performance of the sampled-data deterministic learning algorithm (serving as an example of discrete-time adaptive algorithms), including the learning speed and learning accuracy, by applying the relations of PE level.

4 Relations of PE level for RBF neural networks under the discrete-time framework

In the following section, the relations for the PE level of RBFNN are given. For ease of reading and understanding, Figure 2 briefly shows the relationship between the PE level derived in this section and the properties of the discrete signal and the RBFNN's structure parameters. Here, the neural network is generally considered with the neuron centers uniformly arranged on a regular lattice to cover the compact set Ω, and the input trajectory Z inside Ω is recurrent.

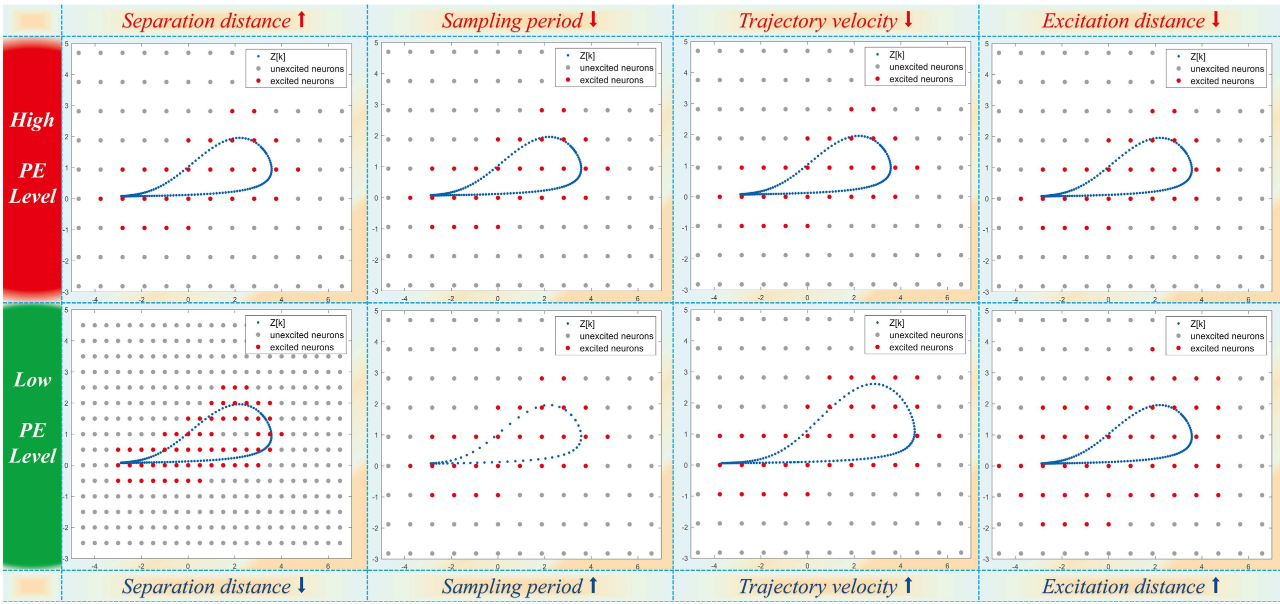

Figure 2 (Color online) Demonstration of some factors that contribute to PE level in the discrete-time framework.

4.1 Relation between PE level, separation distance, and excitation distance

Theorem 1. Consider any trajectory satisfying Assumption 1 and the RBFNN's structure with fixed k_η and k_ε, if $0 < k_\varepsilon \leqslant k_{\varepsilon'}$, the PE level μ increases with increasing separation distance h and satisfies

$$\mu \geqslant c_{\min}^2 c_t \frac{h}{\kappa T_s}, \tag{23}$$

where $c_{\min}$ is a constant independent of the trajectory, c_t is a constant related to the trajectory and k_ε, κ is the maximum trajectory velocity.

Proof. The proof is divided into four steps as follows.

Step 1. The first step is to obtain the general relation for μ by drawing on and combining the proofs in [13,14,20]. Choose the sampling time point set $D = [k', k'+1, \ldots, k'+K-1]$ for a trajectory period. Define subsets D_i as

$$D_i = \{k \in D : \|Z[k] - \xi_i\| \leqslant \varepsilon\},\ i = 1, \ldots, N_\zeta. \tag{24}$$

We divide the time points at which the trajectory Z stays within the intersecting balls to avoid D_i from overlapping. Specifically, D_i is rewritten as

$$D_i = D_{i_0} + D_{i_1} + \cdots + D_{i_Q}, \tag{25}$$

where $1 \leqslant Q \leqslant N_\zeta - 1$, D_{i_0} denotes the time points that trajectory Z visits and only visits the ball with center ξ_i and neighborhood ε (ε-ball), and D_{i_k} ($k = 1, \ldots, Q$) denotes the time points that trajectory Z simultaneously visits and only visits $k+1$ intersecting balls. Note that if $k_\varepsilon \leqslant 1$, then $D_{i_k} = 0, \forall k \geqslant 1$.

Furthermore, we denote

$$D_i' = D_{i_0} + \frac{1}{2} D_{i_1} + \cdots + \frac{1}{Q+1} D_{i_Q}, \tag{26}$$

where $\frac{1}{k+1} D_{i_k}$ ($k = 1, \ldots, Q$) denotes the divided piece of time points that trajectory Z simultaneously visits and only visits the $k+1$ intersecting balls. Thus, the overlapped sets D_i are divided into non-intersecting sets D_i'.

Since $\cup_{i=1}^{N_\zeta} D_i' \subseteq D$, we have

$$\begin{aligned} c^{\mathrm{T}} \left\{ \sum_{k=k'}^{k'+K-1} S_\zeta(Z[k]) S_\zeta^{\mathrm{T}}(Z[k]) \right\} c &= \sum_{k=k'}^{k'+K-1} \left| S_\zeta^{\mathrm{T}}(Z[k]) c \right|^2 \\ &\geqslant \sum_{i=1}^{N_\zeta} \left\{ \sum_{k \in D_i'} \left| S_\zeta^{\mathrm{T}}(Z[k]) c \right|^2 \right\}, \end{aligned} \tag{27}$$

where $c=\left[c_1,\ldots,c_{N_\zeta}\right]^{\mathrm{T}}\in\mathbb{R}^{N_\zeta}$ is an arbitrary unit constant vector.

Then, since $k\in D_i'$ implies that $Z[k]$ in the ball $\|Z[k]-\xi_i\|\leqslant\varepsilon$ and $\left|\sum_{\iota=1}^{N_\zeta}s\left(\|x-\xi_\iota\|\right)c_\iota\right|^2$ is continuous over this compact and connected ball $\|x-\xi_i\|\leqslant\varepsilon$, we apply the mean value theorem to obtain the following:

$$\begin{aligned}\sum_{k\in D_i'}\left|S_\zeta^{\mathrm{T}}\left(Z[k]\right)c\right|^2&=\left|S_\zeta^{\mathrm{T}}\left(Z_i\right)c\right|^2\operatorname{card}\left(D_i'\right)\\&=\left|\sum_{\iota=1}^{N_\zeta}s\left(\|Z_i-\xi_\iota\|\right)c_\iota\right|^2\operatorname{card}\left(D_i'\right),\end{aligned}\tag{28}$$

where $Z_i\in\mathbb{R}^n$ such that $\|Z_i-\xi_i\|\leqslant\varepsilon$. For a finite set, $\operatorname{card}(\cdot)$ denotes the number of elements in the set. Then, we immediately have the ability to scale (27) and obtain the following inequality:

$$\sum_{i=1}^{N_\zeta}\left\{\sum_{k\in D_i'}\left|S_\zeta^{\mathrm{T}}\left(Z[k]\right)c\right|^2\right\}\geqslant\sum_{i=1}^{N_\zeta}\left|\sum_{\iota=1}^{N_\zeta}s\left(\|Z_i-\xi_\iota\|\right)c_\iota\right|^2N_{D_i'},\tag{29}$$

where $N_{D_i'}=\min_i\operatorname{card}\left(D_i'\right)>0$ is used for ease of express.

Furthermore, the inequality (29) imply that

$$\sum_{i=1}^{N_\zeta}\left\{\sum_{k\in D_i'}\left|S_\zeta^{\mathrm{T}}\left(Z[k]\right)c\right|^2\right\}\geqslant\left\|A_\zeta c\right\|^2N_{D_i'},\tag{30}$$

where A_ζ is an $N_\zeta\times N_\zeta$ interpolation matrix and it has the following form:

$$\begin{aligned}A_\zeta&=A_\zeta\left(Z_1,\ldots,Z_{N_\zeta}\right)\\&=\begin{bmatrix}s\left(\|Z_1-\xi_1\|\right)&\ldots&s\left(\left\|Z_1-\xi_{N_\zeta}\right\|\right)\\\vdots&\ddots&\vdots\\s\left(\left\|Z_{N_\zeta}-\xi_1\right\|\right)&\ldots&s\left(\left\|Z_{N_\zeta}-\xi_{N_\zeta}\right\|\right)\end{bmatrix},\end{aligned}\tag{31}$$

where the singularity of A_ζ for the Z_i satisfying $\|Z_i-\xi_i\|\leqslant\varepsilon$ is analysed in detail by [14,20]. It can be concluded that A_ζ is nonsingular for all Z_i if $0<k_\varepsilon\leqslant1$. And based on Lemma 2, A_ζ is nonsingular for a dense subset of Z_i under Assumption 1 if $1<k_\varepsilon\leqslant k_{\varepsilon'}$.

Then, the last inequality (30) can be rewritten as follows:

$$\begin{aligned}\sum_{i=1}^{N_\zeta}\left\{\sum_{k\in D_i'}\left|S_\zeta^{\mathrm{T}}\left(Z[k]\right)c\right|^2\right\}&\geqslant\left\|A_\zeta c\right\|^2N_{D_i'}\\&\geqslant\theta^2\|c\|^2N_{D_i'}\\&=\theta^2N_{D_i'}\\&=\mu,\end{aligned}\tag{32}$$

where θ is the minimum eigenvalue of $A_\zeta^{\mathrm{T}}A_\zeta$ and $\theta>0$.

Step 2. In (32), we obtain the general relation for μ, and in the next step, we first give an exact estimate for θ. We will refer to the proof process of [13] here. First, split A_ζ into its symmetric and antisymmetric parts, $A_\zeta=A_{\zeta\mathrm{sym}}+A_{\zeta\mathrm{anti}}$. Since $c\in\mathbb{R}^{N_\zeta}$ is an arbitrary unit constant vector and by using $c_0^{\mathrm{T}}A_{\zeta\mathrm{anti}}c_0=0$, $\forall c_0\in\mathbb{R}^{N_\zeta}$, we get $c^{\mathrm{T}}A_\zeta c=c^{\mathrm{T}}A_{\zeta\mathrm{sym}}c$. By applying the Cauchy-Schwarz inequality, we have $\|A_\zeta c\|\,\|c\|\geqslant c^{\mathrm{T}}A_{\zeta\mathrm{sym}}c$. Then, the minimum of $\|A_\zeta c\|/\|c\|$ can be got as follows due to A_ζ is a real matrix

$$\frac{\left\|A_\zeta\left(Z_1,\ldots,Z_{N_\zeta}\right)c\right\|}{\|c\|}\geqslant\min_{\|c\|=1}c^{\mathrm{T}}A_{\zeta\mathrm{sym}}\left(Z_1,\ldots,Z_{N_\zeta}\right)c.\tag{33}$$

Rewrite and simplify the symmetric quadratic form on the right above, which yields

$$
\begin{aligned}
&c^{\mathrm{T}} A_{\zeta\mathrm{sym}}\left(Z_1, \ldots, Z_{N_\zeta}\right) c \\
&\quad= c^{\mathrm{T}} A_{\zeta\mathrm{sym}}\left(\xi_1, \ldots, \xi_{N_\zeta}\right) c + \left(c^{\mathrm{T}} A_{\zeta\mathrm{sym}}\left(Z_1, \ldots, Z_{N_\zeta}\right) c - c^{\mathrm{T}} A_{\zeta\mathrm{sym}}\left(\xi_1, \ldots, \xi_{N_\zeta}\right) c\right) \\
&\quad= I_\zeta + J_\zeta,
\end{aligned} \tag{34}
$$

where I_ζ and J_ζ denote the obvious quadratic forms and have the mathematical expression as follows:

$$
I_\zeta = \sum_{j,l=1}^{N_\zeta} c_j c_l s\left(\left\|\xi_j - \xi_l\right\|\right) \tag{35}
$$

and

$$
J_\zeta = \frac{1}{(2\pi)^n} \int_0^\infty \frac{1}{t^{n/2}} \int_{\mathbb{R}^n} \mathrm{e}^{-\frac{\|u\|^2}{4t}} \left[\sum_{j,l=1}^{N_\zeta} c_j c_l \mathrm{e}^{-\mathrm{i}(\xi_j - \xi_l)u} \left(1 - \mathrm{e}^{-\mathrm{i}d_j u}\right)\right] \mathrm{d}u \mathrm{d}\mathcal{U}(t), \tag{36}
$$

where the parameters in the equations are replaced with those used in this paper. The detailed derivation of the above conclusion is rigorously presented in the proof of Theorem 3.2 (specifically, equation (3.5)) in [36].

Since $s(\cdot) = \exp\left(-\|\cdot\|^2/\eta^2\right)$ is the Gaussian function, the measure $\mathrm{d}\mathcal{U}(t) = \delta\left(t - 1/\eta^2\right)$ is used to represent the scaled Gaussian $s(\cdot)$. Then, from (36), we obtain

$$
J_\zeta = \frac{\eta^n}{(2\pi)^n} \int_{\mathbb{R}^n} \mathrm{e}^{-\frac{\|u\|^2 \eta^2}{4}} \left[\sum_{j,l=1}^{N_\zeta} c_j c_l \mathrm{e}^{-\mathrm{i}(\xi_j - \xi_l)u} \left(1 - \mathrm{e}^{-\mathrm{i}d_j u}\right)\right] \mathrm{d}u. \tag{37}
$$

By scaling (34), it yields the lower bound of θ:

$$
\begin{aligned}
\theta &= \min_{\|c\|=1} c^{\mathrm{T}} A_{\zeta\mathrm{sym}}\left(Z_1, \ldots, Z_{N_\zeta}\right) c \\
&= \min\left(I_\zeta + J_\zeta\right) \\
&\geqslant I_\zeta - \left|J_\zeta\right|.
\end{aligned} \tag{38}
$$

By rewriting and extending the proof of Proposition 3.12 in [36] (see Appendix A), the absolute value of J_ζ satisfies the following upper bound:

$$
\begin{aligned}
\left|J_\zeta\right| &\leqslant \sum_{j=1}^{N_\zeta} \left|c_j\right|^2 \left|\left(\nabla_{d_j} F\right)(0)\right| + \sum_{j,l=1}^{N_\zeta}{}' \left|c_j c_l\right| \left|\left(\nabla_{d_j} F\right)\left(\xi_l - \xi_j\right)\right| \\
&=: \mathbb{S}_1 + \mathbb{S}_2,
\end{aligned} \tag{39}
$$

where $\sum'$ in (39) indicates that $j \neq l$ in that sum. The upper bound of $\mathbb{S}_1$ can be directly provided:

$$
\mathbb{S}_1 \leqslant \frac{\varepsilon^2}{\eta^2} \|c\|^2 = \frac{\varepsilon^2}{\eta^2}. \tag{40}
$$

While the upper bound of $\mathbb{S}_2$ is related to k_ε. If $0 < k_\varepsilon \leqslant 2$ (i.e., $0 < \varepsilon \leqslant 2h$),

$$
\mathbb{S}_2 \leqslant \frac{6nh\varepsilon}{\eta^2} \sum_{i=1}^{\infty} (i+2)^{n-1} (i+3) \mathrm{e}^{-\frac{(i-2)^2 h^2}{\eta^2}}. \tag{41}
$$

And if $2 < k_\varepsilon \leqslant k_{\varepsilon'}$ (i.e., $2h < \varepsilon \leqslant \varepsilon'$),

$$
\mathbb{S}_2 \leqslant \frac{6nh\varepsilon}{\eta^2} \sum_{i=1}^{\left\lfloor \frac{\varepsilon}{2h} \right\rfloor} (i+2)^{n-1} \left[i + 1 + \frac{\varepsilon}{h}\right] \mathrm{e}^{-\frac{i^2 h^2}{\eta^2}} + \frac{6nh\varepsilon}{\eta^2} \sum_{i=1}^{\infty} (i+2)^{n-1} \left[i + 1 + \frac{\varepsilon}{h}\right] \mathrm{e}^{-\frac{\left(i - \frac{\varepsilon}{h}\right)^2 h^2}{\eta^2}}. \tag{42}
$$

By summing the upper bounds of $\mathbb{S}_1$ and $\mathbb{S}_2$, we obtain the following:

$$|J_\zeta| \leqslant \begin{cases} \dfrac{k_\varepsilon^2}{k_\eta^2} + 6n\dfrac{k_\varepsilon}{k_\eta^2} f_1\left(\dfrac{1}{k_\eta^2}\right), & 0 < k_\varepsilon \leqslant 2, \\ \dfrac{k_\varepsilon^2}{k_\eta^2} + 6n\dfrac{k_\varepsilon}{k_\eta^2} f_2\left(\dfrac{1}{k_\eta^2}\right), & 2 < k_\varepsilon \leqslant k_{\varepsilon'}, \end{cases} \tag{43}$$

where $f_1(x) = \sum_{i=1}^{\infty} (i+2)^{n-1} (i+3) \mathrm{e}^{-(i-2)^2 x}$ and $f_2(x) = \sum_{i=1}^{\lfloor \frac{k_\varepsilon}{2} \rfloor} (i+2)^{n-1} (i+1+k_\varepsilon) \mathrm{e}^{-i^2 x} + \sum_{i=1}^{\infty} (i+2)^{n-1} \times (i+1+k_\varepsilon) \mathrm{e}^{-(i-k_\varepsilon)^2 x}$.

Besides, we obtain the following estimate for I_ζ from Example 2.6 in [43]:

$$I_\zeta \geqslant C(n) \left(\frac{\eta}{h}\right)^n \mathrm{e}^{-\frac{\sigma^2 \eta^2}{h^2}}, \tag{44}$$

where $C(n)$ and σ are constants given by

$$C(n) = \frac{n^{\frac{n}{2}} \pi^{\frac{5n}{2}}}{2^{4n-1}(n+2)}, \quad \sigma = \frac{(n+1)\pi}{4}. \tag{45}$$

Finally, by combining (43) and (44), the lower bound of θ is given as follows:

$$\theta \geqslant \begin{cases} C(n)\left(\dfrac{\eta}{h}\right)^n \mathrm{e}^{-\frac{\sigma^2\eta^2}{h^2}} - \dfrac{k_\varepsilon^2}{k_\eta^2} - 6n\dfrac{k_\varepsilon}{k_\eta^2} f_1\left(\dfrac{1}{k_\eta^2}\right), & 0 < k_\varepsilon \leqslant 2, \\ C(n)\left(\dfrac{\eta}{h}\right)^n \mathrm{e}^{-\frac{\sigma^2\eta^2}{h^2}} - \dfrac{k_\varepsilon^2}{k_\eta^2} - 6n\frac{k_\varepsilon}{k_\eta^2} f_2\left(\dfrac{1}{k_\eta^2}\right), & 2 < k_\varepsilon \leqslant k_{\varepsilon'}. \end{cases} \tag{46}$$

Step 3. In the above step, we have obtained the exact estimate for θ, and in the third step, we proceed to give an approximate estimate for $N_{D_i'}$. From the discrete-time version of the PE definition, $N_{D_i'}$ denotes the minimum number of sampling points in the time spent in an ε-ball about each of the neurons and is dependent on the dynamical system input trajectory Z. By considering the maximum trajectory velocity κ and the sampling period T_s, we can estimate the number of sampling points contained within a ε-ball when the trajectory penetrates the ball with the maximum velocity κ,

$$N_0 = \frac{c_t' \varepsilon}{T_s \kappa}, \tag{47}$$

where c_t' is a constant determined by the specific trajectory.

By considering that the neurons are uniformly arranged, with each neuron occupying a space of volume h^n, we give an estimate of the number of nearby neurons that can be excited at a sampling point.

$$N_a = \frac{V(\varepsilon)}{h^n}, \tag{48}$$

where $V(r) = \frac{\pi^{\frac{n}{2}}}{\Gamma\left(\frac{n}{2}+1\right)} r^n$ denotes the volume of an n-dimensional ball of radius r.

Then, the $N_{D_i'}$ can be estimated as

$$N_{D_i'} = \frac{N_0}{N_a} = \frac{c_t' \Gamma\left(\frac{n}{2}+1\right) h^n}{\pi^{\frac{n}{2}} T_s \kappa \varepsilon^{n-1}}. \tag{49}$$

For ease of express, we rewrite the (49) to obtain

$$N_{D_i'} = c_t \frac{h}{\kappa T_s}, \tag{50}$$

with $c_t = \frac{c_t' \Gamma\left(\frac{n}{2}+1\right)}{\pi^{\frac{n}{2}} k_\varepsilon^{n-1}}$ is a constant.

Step 4. In the two steps above, estimates have been derived for θ and $N_{D_i'}$, thus enabling us to provide an estimate for μ. By fixing k_η and k_ε, then

$$\theta \geqslant \begin{cases} C(n) k_\eta^n \mathrm{e}^{-\sigma^2 k_\eta^2} - \dfrac{k_\varepsilon^2}{k_\eta^2} - 6n\dfrac{k_\varepsilon}{k_\eta^2} f_1\left(\dfrac{1}{k_\eta^2}\right), & 0 < k_\varepsilon \leqslant 2, \\ C(n) k_\eta^n \mathrm{e}^{-\sigma^2 k_\eta^2} - \dfrac{k_\varepsilon^2}{k_\eta^2} - 6n\dfrac{k_\varepsilon}{k_\eta^2} f_2\left(\dfrac{1}{k_\eta^2}\right), & 2 < k_\varepsilon \leqslant k_{\varepsilon'}. \end{cases} \tag{51}$$

With fixed k_ε, k_η and the input trajectory dimension n, all factors in (51) become constants. We have reason to choose the positive constants C_1 and C_2 such that

$$\begin{aligned} C_1 &\geqslant C\left(n\right) k_\eta^n \mathrm{e}^{-\sigma^2 k_\eta^2} - \frac{k_\varepsilon^2}{k_\eta^2} - 6n\frac{k_\varepsilon}{k_\eta^2} f_1\left(\frac{1}{k_\eta^2}\right), \\ C_2 &\geqslant C\left(n\right) k_\eta^n \mathrm{e}^{-\sigma^2 k_\eta^2} - \frac{k_\varepsilon^2}{k_\eta^2} - 6n\frac{k_\varepsilon}{k_\eta^2} f_2\left(\frac{1}{k_\eta^2}\right). \end{aligned} \tag{52}$$

Finally, the general relation for μ with respect to h, obtained by combining (50)–(52) is as follows:

$$\begin{aligned} \mu &\geqslant \begin{cases} C_1^2 c_t \dfrac{h}{\kappa T_s}, & 0 < k_\varepsilon \leqslant 2, \\ C_2^2 c_t \dfrac{h}{\kappa T_s}, & 2 < k_\varepsilon \leqslant k_{\varepsilon'} \end{cases} \\ &\geqslant c_{\min}^2 c_t \frac{h}{\kappa T_s}, \quad 0 < k_\varepsilon \leqslant k_{\varepsilon'}, \end{aligned} \tag{53}$$

where $c_{\min} = \min\left\{C_1, C_2\right\}$.

Remark 3. Note that the definition of PE shows that the PE level will have an upper bound KS_m^2. This shows that (23) in Theorem 1 implies that as h increases, μ increases and tends to the upper bound of the PE level rather than growing indefinitely.

Remark 4. From the proof of Theorem 1, c_t is a constant determined by the input trajectory and is fixed when the trajectory is known *a priori*. It can be seen that the PE level μ is related to the maximum trajectory velocity κ and sampling period T_s. As κ increases, the number of sampling points in the time spent in an ε-ball about the neuron decreases and the minimum number of sampling points $N_{D_i'}$ also decreases, then the PE level μ decreases. As T_s increases, μ decreases for the same reason that μ decreases due to an increase in κ. The above conclusion is based on our estimates of $N_{D_i'}$, and the effectiveness of the estimate is shown in the simulation section.

Theorem 2. Consider any trajectory satisfying Assumption 1 and the RBFNN's structure with fixed k_η and the separation distance h, if $0 < k_\varepsilon \leqslant k_{\varepsilon'}$, the PE level μ decreases as the excitation distance ε increases.

Proof. Fixing h to increase ε implies that k_ε increases, and in (50) and (51) we can see that $N_{D_i'}$ and θ decrease as k_ε increases. Thus, with k_η and separation distance h fixed, μ decreases as ε increases.

Remark 5. As the excitation distance ε increases, neurons further away from the input trajectory are excited, causing the trajectory time spent in an ε-ball about the neuron to be split between more neurons, and $N_{D_i'}$ decreases.

4.2 Relation between PE level and receptive field width

Theorem 3. Consider any trajectory satisfying Assumption 1 and the RBFNN's structure with fixed separation distance h and k_ε, if $k_\eta \geqslant \sqrt{\frac{8n}{\pi^2(n+1)^2}}$, the PE level μ decreases as the receptive field width η of the neuron increases, while if $k_\eta < \sqrt{\frac{8n}{\pi^2(n+1)^2}}$, the PE level μ decreases with decreasing receptive field width η.

Proof. From the proof of Theorem 1, by observing (32) and (38), we can obtain that

$$\mu = \theta^2 N_{D_i'} \tag{54}$$

and

$$\theta \geqslant I_\zeta - \left|J_\zeta\right|. \tag{55}$$

Let k_ε and the separation distance h be fixed. Then μ is only proportional to θ.

Then, the estimate for I_ζ is provided in (44) as follows:

$$I_\zeta \geqslant C\left(n\right) k_\eta^n \mathrm{e}^{-\sigma^2 k_\eta^2}, \tag{56}$$

where $C\left(n\right)$ is a constant and $\sigma = \frac{(n+1)\pi}{4}$.

From (56), the derivative of I_ζ with respect to h satisfies

$$\frac{\partial I_\zeta}{\partial k_\eta} = -C\left(n\right) k_\eta^{n-1}\left(2\sigma^2 k_\eta^2 - n\right) \mathrm{e}^{-\sigma^2 k_\eta^2}. \tag{57}$$

Let $\frac{\partial I_\zeta}{\partial k_\eta}=0$ and $\sigma=\frac{(n+1)\pi}{4}$, then we have

$$\begin{cases} \dfrac{\partial I_\zeta}{\partial k_\eta}>0, \quad k_\eta\in\left(0,\sqrt{\dfrac{8n}{\pi^2(n+1)^2}}\right), \\ \dfrac{\partial I_\zeta}{\partial k_\eta}=0, \quad k_\eta=\sqrt{\dfrac{8n}{\pi^2(n+1)^2}}, \\ \dfrac{\partial I_\zeta}{\partial k_\eta}<0, \quad k_\eta\in\left(\sqrt{\dfrac{8n}{\pi^2(n+1)^2}},\infty\right). \end{cases} \tag{58}$$

Here, we consider $|J_\zeta|$ as a perturbation to θ to simplify the proof, which is that θ is dominated by I_ζ. Then, when $k_\eta\geqslant\sqrt{\frac{8n}{\pi^2(n+1)^2}}$, An increase in η causes I_ζ to decrease resulting in leads to a decrease in $I_\zeta-|J_\zeta|$, while when $k_\eta<\sqrt{\frac{8n}{\pi^2(n+1)^2}}$, A decrease in η causes I_ζ to decrease resulting in a decrease in $I_\zeta-|J_\zeta|$ and both of two cases result in a decrease in θ and eventually in μ, which ends the proof.

Remark 6. It can be seen that there will exist an optimal value η^* to obtain the maximum PE level. However, the η^* may deviate slightly from $\sqrt{\frac{8n}{\pi^2(n+1)^2}}$ due to the existence of the perturbation $|J_\zeta|$ not considered yet in the proof. The relation obtained based on the above consideration is demonstrated in the simulation section.

In the above theorems, the relationships between separation distance h, excitation distance ε, receptive field width η, and the PE level μ are given for the discrete-time version, which relates not to the framework of the specific algorithm. When the input trajectories satisfy Assumption 1, the obtained relations of PE level can be applied for performance analysis by a large class of algorithms that are based on RBFNN for adaptive control, identification, and learning of the sampling system.

5 Performance analysis for deterministic learning under sampled-data framework

In the following analysis, we apply the relations of the PE level obtained above to the algorithm for sampled-data deterministic learning and use the PE level as a bridge to explore the close relationships between the performance of the learning algorithm and the RBFNN's structure parameters for optimal algorithm performance.

5.1 Performance analysis based on separation distance

Based on the explicit convergence relation for the learning error system (18) established in Lemma 3, for performance analysis, we first analyze the learning speed by using the convergence rate σ (20).

Corollary 1 (Learning speed)**.** Consider the learning error system (18) with fixed k_η and k_ε, if $0<\alpha_i\leqslant\omega_i$ and $\frac{1}{\alpha_i}\leqslant\gamma\leqslant\frac{1}{2T_s^2S_m^2}$ under Assumption 1, the convergence rate σ decreases as the separation distance h increases.

Proof. According to the Lemma 3, we take (23) into the ω_i to obtain that

$$\omega_i=\left(1-\frac{2KT_s\gamma\left(2-S_m^2T_s^2\gamma\right)c_{\min}^2c_th\kappa^{-1}}{(K-1)KS_m^4T_s^4\gamma^2+2\left(KS_m^2-1\right)T_s^2\gamma+2}\right)^{\frac{1}{2K}}. \tag{59}$$

From (20) and (59), the derivative of σ with respect to h yields

$$\frac{\partial\sigma}{\partial h}=\frac{\omega_i}{\sigma}\frac{\partial\omega_i}{\partial h}=\frac{-m\omega_i}{2K\sigma}\left(1-mh\right)^{\frac{1}{2K}-1}<0, \tag{60}$$

where $m=\frac{2KT_s\gamma\left(2-S_m^2T_s^2\gamma\right)c_{\min}^2c_t\kappa^{-1}}{(K-1)KS_m^4T_s^4\gamma^2+2(KS_m^2-1)T_s^2\gamma+2}\in\mathbb{R}_+$ is a constant. From (60), it can be deduced that σ is inversely proportional to h.

Remark 7. Based on the PE level, we obtained the relationship between the separation distance of RBFNN and learning speed, revealing that constructing an appropriate neural network structure may contribute to the performance of the algorithm.

Then, we analyze the learning accuracy by using the convergence bound b (21).

Corollary 2 (Learning accuracy). Consider the learning error system (18) with fixed k_η and k_ε, if $0<\alpha_i\leqslant\omega_i$, $\frac{1}{\alpha_i}\leqslant\gamma\leqslant\frac{1}{2T_s^2S_m^2}$ and $\sqrt{n}\leqslant k_\varepsilon\leqslant k_{\varepsilon'}$ under Assumption 1, there exists an optimal separation distance h^* that minimizes the convergence bound b.

Proof. The proof is divided into three steps as follows.

Step 1. From Lemma 1, the $\bar{\epsilon}_{\zeta i}$ in (21) is replaced by $\bar{\epsilon}_{\zeta i}(h_{\Xi,\Omega})$ and from Theorem 2 in [26], it satisfies

$$\bar{\epsilon}_{\zeta i}(h_{\Xi,\Omega})=\|\epsilon_{\zeta i}[k]\|_{\ell_\infty(X)}. \tag{61}$$

From (61), we first analyse $\bar{\epsilon}_{\zeta i}(h_{\Xi,\Omega})$ and give an estimate for it based on Lemma 1.

By letting $\alpha=0$, the $\ell_p(X)$-derivative norms is replaced to the discrete ℓ_p norms. Then, the upper bound of the discrete approximation error $\|\epsilon_{\zeta i}[k]\|_{\ell_\infty(X)}$ is obtained by setting $q=\infty$. Furthermore, $(h_{X,\Omega}/h_X)^{\frac{n}{q}}=1$ if $q=\infty$.

Thus, for RBFNN, its upper bound of discrete approximation error satisfies

$$\|\epsilon_{\zeta i}[k]\|_{\ell_\infty(X)}\leqslant k_1h_{\Xi,\Omega}^{\tau-\frac{n}{2}}\|f\|_{W_2^\tau(\Omega)}, \tag{62}$$

where $\|f\|_{W_2^\tau(\Omega)}\in\mathbb{R}_+$ is a constant dependent on τ and $k_1\in\mathbb{R}_+$ is a constant dependent on q.

Note that the fill distance $h_{\Xi,\Omega}$ is not only related to the input trajectory but also to the separation distance h and the excitation distance ε of RBFNN. Therefore, to determine the general relation between the approximation error and the RBFNN's structure parameters, it is necessary to exclude the influence of the input trajectory.

Step 2. Consider the neurons are uniformly arranged inside the compact set Ω with separation distance h. By setting $\varepsilon\geqslant\sqrt{n}h$, we obtain that

$$h_{\Xi,\Omega}\leqslant\sqrt{n}h \tag{63}$$

and from (62), the upper bound of the discrete approximation error satisfies

$$\|\epsilon_{\zeta i}[k]\|_{\ell_\infty(X)}\leqslant c_bh^{\tau-\frac{n}{2}}, \tag{64}$$

where $c_b=k_1n^{\frac{\tau}{2}-\frac{n}{4}}\|f\|_{W_2^\tau(\Omega)}$ is a constant independent of h.

Here, $\varepsilon\geqslant\sqrt{n}h$ ensures that the input trajectory is completely inside the ε-neighborhood of its nearby neurons, avoiding data loss and deterioration of approximation error caused by the inability of the input data to excite the neuron.

Step 3. Based on the above steps, we can next establish the relation between the convergence bound b and the separation distance h. And due to the complexity of b, before analysing, we first consider b as two parts, b_a and $\|\epsilon_{\zeta i}[k]\|_{\ell_\infty(X)}$,

$$b=\frac{T_s\sqrt{1+\frac{\gamma}{2}}\|\epsilon_{\zeta i}[k]\|_{\ell_\infty(X)}}{(1-\sigma)\sqrt{1-\omega_i^2}}=b_a\|\epsilon_{\zeta i}[k]\|_{\ell_\infty(X)}. \tag{65}$$

(i) We first analyse the relation between b_a and separation distance h. From (59) and (65), evaluating the derivative of b_a with respect to h and combining (60) yields

$$\frac{\partial b_a}{\partial h}=\frac{T_s\sqrt{1+\frac{\gamma}{2}}\frac{\partial\sigma}{\partial h}}{(1-\sigma)^2\sqrt{1-\omega_i^2}}-\frac{T_s\sqrt{1+\frac{\gamma}{2}}m\omega_i(1-mh)^{\frac{1}{2K}-1}}{2K(1-\sigma)(1-\omega_i^2)^{\frac{3}{2}}}<0, \tag{66}$$

which can be inferred from (66) that b_a is inversely proportional to the h.

Then, by observing b_a, it is clear that there exist two poles $h=h_\sigma$ and $h=h_{\omega_i}$, which are obtained when $\sigma=1$ and $\omega_i=1$, respectively. Furthermore, $\sigma>\omega_i$ can be obtained by (20). Then, by solving $\omega_i=1$, we can obtain that $h_{\omega_i}=0$. Since finding an explicit solution for $\sigma=1$ is challenging, we do not intend to obtain the exact value for h_σ, but we can still infer that $h_\sigma>h_{\omega_i}=0$ from $\sigma>\omega_i$. Thus, when separation distance h decreases to h_σ, b_a increases to infinity.

On the other hand, from (66), b_a decreases as h increases. However, b_a does not decrease to 0. By observing (65), it can be obtained that b_a and h are related with σ, ω_i as intermediate variables. According to (60), σ, ω_i decrease as h increases. Then, when σ, ω_i decrease and tend to 0, b_a decreases and tends to the lower bound $T_s\sqrt{1+\frac{\gamma}{2}}$.

(ii) By combining (64) and (65), we have

$$b=c_bb_ah^{\tau-\frac{n}{2}}. \tag{67}$$

According to (i), when the separation distance h decreases and tends to h_σ, b_a increases and tends to infinity while $h^{\tau-\frac{n}{2}}$ decreases to $h_\sigma^{\tau-\frac{n}{2}} \neq 0$. Then, b still tends to be sufficiently large. When the separation distance h increases, b_a decreases and tends to $T_s\sqrt{1+\frac{\gamma}{2}}$ while $h^{\tau-\frac{n}{2}}$ increases. Then, b also increases to be sufficiently large. Hence, we have reason to infer that there exists an optimal separation distance h^* that minimizes b.

Remark 8. Here, we consider the b_a in (65) to represent the ability of the learning algorithm to weaken the approximation error $\|\epsilon_{\zeta i}[k]\|_{\ell_\infty(X)}$. As b_a gets smaller, this ability gets larger; as b_a gets larger, this ability gets smaller, and it may even have a detrimental effect on the approximation error, making it worse. Thus, b_a leads to the trade-off relation between the PE level and the RBFNN's approximation ability. When the PE level is too low, b_a increases rapidly, leading to an obvious deterioration in learning accuracy. Furthermore, although the PE level increases with h, there exists a lower bound $T_s\sqrt{1+\frac{\gamma}{2}}$ on b_a, which is determined by the algorithm's learning gain γ and sampling period T_s. Hence, when the approximation error increases with h, it still leads to a significant deterioration of the learning accuracy. The trade-off relation is demonstrated in the simulation section.

5.2 Performance analysis based on receptive field width

In the following subsection, by considering any trajectory satisfying Assumption 1 and the RBFNN's structure with fixed separation distance h and k_ε, we briefly qualitatively analyze the effect of the receptive field width η of the radial basis function on the learning performance.

Consider the following process for approximating an unknown nonlinear function $f(x)$ using the RBFNN

$$\begin{aligned} f(Z[k]) &= W_\zeta^{\mathrm{T}} S_\zeta(Z[k]) \\ &= \sum_{i=1}^{N_\zeta} w_i s(\|Z[k]-\xi_i\|), \end{aligned} \tag{68}$$

which is characterized as simply computing the NN weights $W_\zeta = \left[w_1,\ldots,w_{N_\zeta}\right]^{\mathrm{T}} \in \mathbb{R}^{N_\zeta}$ as the solution of the linear system

$$\mathcal{A}W_\zeta = \mathrm{f}, \tag{69}$$

where $Z[k] \in \mathbb{R}^n$ is the discrete-time input vector, $\mathrm{f} = [f(Z[1]),\ldots,f(Z[M])]^{\mathrm{T}} \in \mathbb{R}^M$ consists of M sampling points of $f(x)$ and the $\mathcal{A}$ has the matrix entries $\mathcal{A}_{j,k} = s(\|Z[j]-\xi_k\|)$.

When the receptive field width η increases, the radial basis function becomes increasingly "flat", and according to [44], the matrix $\mathcal{A}$ becomes very ill-conditioned. Thus, the magnitude of the w_i values becomes considerably large, with some being positive and others negative. Then, when $f(Z[k])$ of size $O(1)$ is obtained in (68) by combining these large quantities, a massive numerical cancellation occurs. Obviously, the two numerically unstable ill-conditioned steps (68) and (69) (called the RBF-direct method) lead to an increase in the approximation error of the RBFNN. Although the numerical instabilities of the RBF-direct method can be avoided or bypassed by many methods, such as RBF-QR [44] and Contour-Pade [45], this paper still focuses on the RBF-direct method for ease of following discussion. Thus, we obtain that when η increases, the approximation error of the RBFNN also increases, while according to Theorem 3, the PE level decreases, then the lower PE level and the larger approximation error simultaneously lead to a decrease in the learning accuracy.

On the other hand, when the receptive field width η decreases, the radial basis function becomes "narrower" and "sharper", resulting in a reduction in the area that can excite the neuron. Consequently, there are parts of the input trajectory Z where neurons in its neighborhood are not excited, and furthermore (68) is rewritten as follows:

$$f(Z[k]) = \sum_{i=1}^{N'_\zeta} w_i s(\|Z[k]-\xi_i\|), \tag{70}$$

where $N'_\zeta < N_\zeta$. Obviously, as η decreases, the number of excited neurons decreases, which leads to fewer dimensions in the approximation space and fewer dimensions in the solution vector $W_\zeta \in \mathbb{R}^{N'_\zeta}$. Due to the inherent difficulty of capturing the nuances and complexity of the objective function $f(x)$, a lower-dimensional approximation space may inevitably lead to an increase in the approximation error. Additionally, if the sampling points do not coincide with the neuron centers, the matrix $\mathcal{A}$ may again become ill-conditioned. Consequently, when η decreases, the larger approximation error and the lower PE level (obtained by Theorem 3) again decrease the learning accuracy.

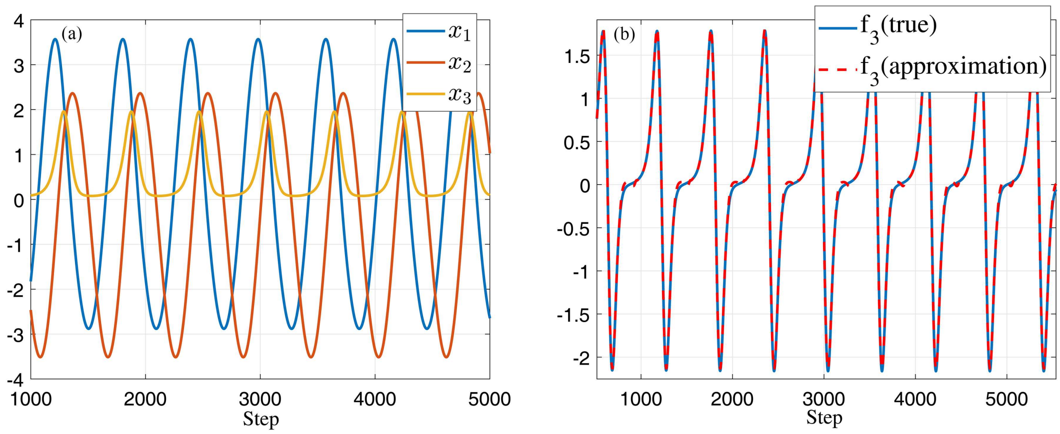

Figure 3 (Color online) (a) Rössler system states: x_1, x_2, x_3; (b) function approximation of f_3.

Remark 9. It can be inferred that when the receptive field width η decreases or increases, the approximation error will increase for different reasons, that is, there is an optimal value η_e^* to minimize the approximation error. Further, based on Theorem 3, we have an optimal value η^* to obtain the maximum PE level. Thus, we infer that there is an optimal value of η_{acc}^* to maximize the learning accuracy of sampled-data deterministic learning using the RBF-direct method. Support is provided in the simulation section.

Remark 10. In the past, there have been a number of successful practical applications of deterministic learning. Based on the accurate modeling of inherent dynamics, control performance is enhanced in similar control tasks [21, 22], and dynamical patterns can be effectively represented and distinguished in the recognition tasks [23, 24, 46]. Furthermore, deterministic learning-based modeling can also be applied to more complex tasks in distributed situations [47–50]. The effectiveness of the above applications cannot be achieved without a high requirement for deterministic learning-based modeling performance, which is the starting point of our work. In this paper, the obtained PE level relations for RBF neural networks are applied to the performance analysis of a deterministic learning algorithm. We demonstrate the existence of an optimal network separation distance and receptive field width, which maximize the learning accuracy, respectively. Subsequently, the algorithmic improvement of deterministic learning in practical applications will be the focus topic.

6 Simulation

In this section, the classical chaotic system (Rössler system [51]) common in nonlinear dynamics is presented to verify the proposed explicit relation for PE level and to demonstrate the results of this relation applied to the performance analysis of deterministic learning:

$$\begin{aligned} \dot{x}_1 &= -x_2 - x_3, \\ \dot{x}_2 &= x_1 + p_1 x_2, \\ \dot{x}_3 &= p_2 + x_3 \left(x_1 - p_3\right), \end{aligned} \tag{71}$$

where $x = [x_1, x_2, x_3]^{\mathrm{T}}$ denotes the system state vector, $p_s = [p_1, p_2, p_3]^{\mathrm{T}}$ denotes the constant vector of system parameters. Here, we consider the sampling data $Z[x_0, T_s, N] = [x[t_0], x[t_0 + T_s], \ldots, x[t_0 + NT_s]]^{\mathrm{T}}$ with sampling period T_s generated from Rössler system.

According to [52], $p_s = [0.2, 0.4, 2.4]^{\mathrm{T}}$ is chosen to yield the Rössler system trajectory (see Figure 3(a)). We consider that the nonlinear system $f_3(x_1, x_3) = p_2 + x_3(x_1 - p_3)$ is unknown. The system state is then initialized to $x[t_0] = [0, 0, 0]^{\mathrm{T}}$ and the sampling period is set to $T_s = 0.01$. The function approximation of f_3 from deterministic learning is given in Figure 3(b). Since the trajectory region of the input system states x_1 and x_3 have been determined, the region where the neurons are arranged is set to $[-4, 4] \times [-4, 4]$. The RBFNN's structure parameters are initialized and set to default values as follows: $h = 0.5$, $k_\varepsilon = 1.5$, and $k_\eta = 1$.

By fixing k_η, from Figure 4(a), it can be seen that both PE level μ and h are linearly proportional at different k_ε, and the proportion decreases with increasing k_ε, showing the effectiveness of the proof that PE levels remain a linearly proportional relation under different k_ε. Then, with fixed k_η and k_ε, by setting different sampling periods T_s, Figure 4(b) shows that the PE level increases proportionally with decreasing T_s proportionally. It shows that

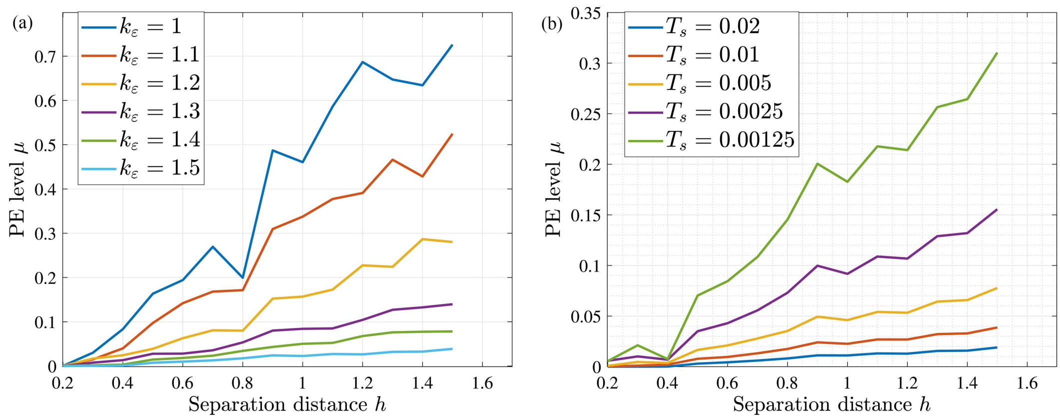

Figure 4 (Color online) Relation between PE level μ and separation distance h for different (a) k_ε and (b) T_s.

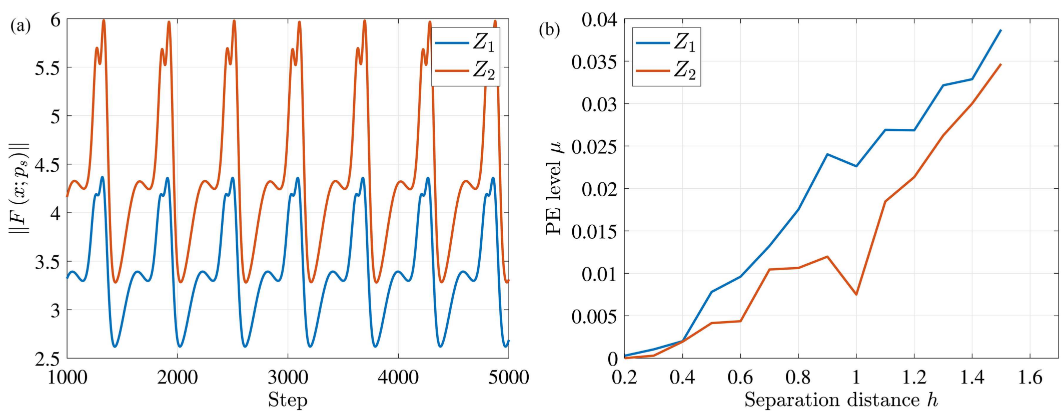

Figure 5 (Color online) (a) Comparison of velocities $\|F(x;p_s)\|$ under different trajectories Z_1 and Z_2; (b) relation between PE level μ and separation distance h under different velocities.

Table 2 Relations from the RBFNN's structure parameters and input trajectory to PE level.

Variable	Relation to PE level μ
Separation distance h	Linearly proportional
Excitation distance ε	Inversely proportional
Receptive field width η	Existence of optimal values
Sampling period T_s	Linearly and inversely proportional
Trajectory velocity κ	Inversely proportional

PE level μ and sampling period T_s are linearly and inversely proportional. Moreover, by fixing $p_1 = 0.2$, $p_2 = 0.4$, let $p_3 = 2.4$ and $p_3 = 3$ to respectively yield two trajectories Z_1, Z_2 with different velocities $\|F(x;p_s)\| \leqslant \kappa$, and the velocity of trajectory Z_2 is larger than that of trajectory Z_1 (see Figure 5(a)). It can be seen that the PE level of trajectory Z_2 is lower than that of trajectory Z_1 (see Figure 5(b)). It shows that PE level μ and trajectory velocity κ are inversely proportional.

Note that the recurrent trajectory includes a large class of trajectories, and that parameter $p_s = [0.2, 0.4, 2.4]^{\mathrm{T}}$ generates only the period-1 orbit. Here we consider setting parameter $p_s = [0.3, 0.4, 2.4]^{\mathrm{T}}$ to generate period-2 orbit, and setting parameter $p_s = [0.2, 0.2, 4.5]^{\mathrm{T}}$ to generate chaos orbit. Figure 6(a) shows that PE level μ and h are linearly proportional for different orbits. By fixing separation distance h and k_η, the relations from k_ε to PE level are shown in Figure 6(b). It shows that the PE level decreases with the increasing excitation distance ε for different orbits. Further, by fixing h and k_ε, the relations from k_η to PE level are shown in Figure 6(c). For different orbits, the result shows that there exists an optimal receptive field width to maximize the PE level. In Table 2, the relations from the RBFNN's structure parameters and input trajectory to the PE level are summarized in detail.

From Figure 7(a), for different orbits, there exists an optimal separation distance h^* that minimizes the convergence bound b and maximizes learning accuracy. The results are caused by the trade-off between the PE level and the approximation ability of the RBFNN. When h decreases, the lower PE level makes b_a increase rapidly

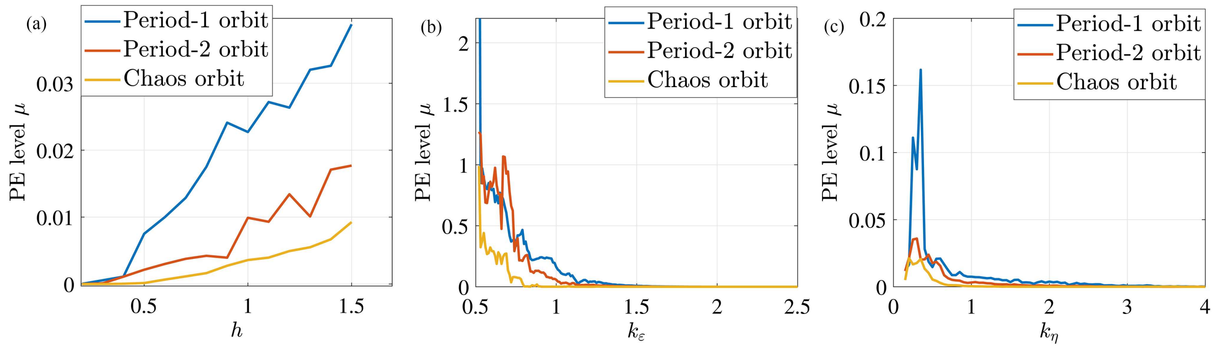

Figure 6 (Color online) Relations between (a) h, (b) k_ε, (c) k_η and PE level μ with different orbits.

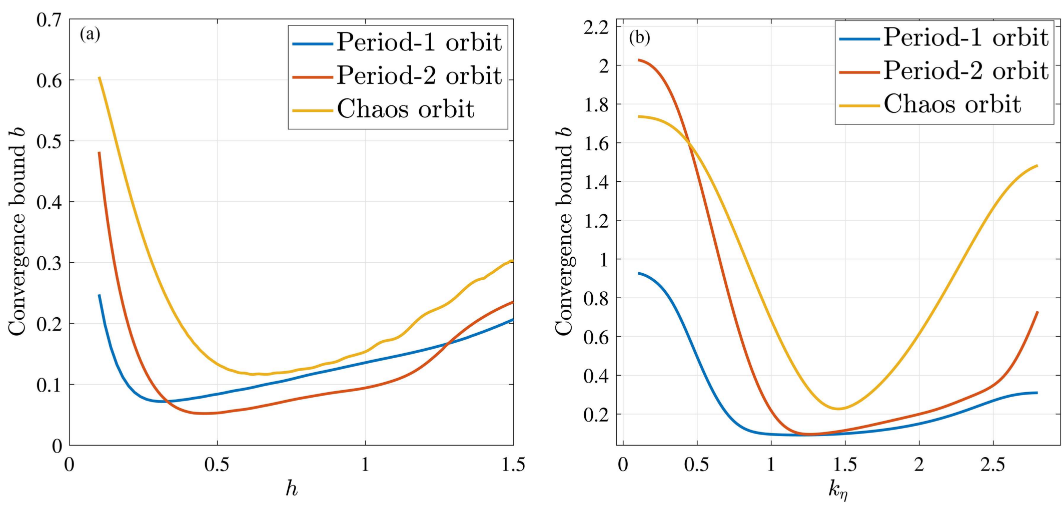

Figure 7 (Color online) Relations between (a) h, (b) k_η and convergence bound b with different orbits.

and decreases the learning accuracy, while when h increases, the increasing PE level is not enough to make the increasing approximation error decrease, so the learning accuracy still decreases. Additionally, for different orbits, our sloppy conclusion that there exists an optimal receptive field width η^*_{acc} to maximize the learning accuracy is also verified in Figure 7(b). This suggests that η also plays an important role in improving learning accuracy.

7 Conclusion

In this paper, the explicit relations for the PE level of RBFNN under the discrete-time framework have been obtained, showing that the PE level increases with increasing separation distance and decreasing sampling period of the input trajectory, respectively, and that larger input trajectory velocity may lead to a smaller excitation level. Subsequently, it has been proven that the PE level decreases with increasing excitation distance, and there exists an optimal receptive field width enabling the highest PE level. The above relations provide significant guidance for the study and improvement of the performance of discrete-time algorithms based on RBFNN. As exemplified by the performance of deterministic learning under a sampled-data framework, including learning speed and learning accuracy, the analysis results have shown that the learning speed is slower as the separation distance decreases. Meanwhile, the existence of an optimal separation distance and an optimal receptive field width has been found to result in maximum learning accuracy, respectively, with the former arising from a trade-off between the approximation ability of the neural network and the excitation level, while the latter is due to the severe ill-conditioning of the interpolation matrix and the approximation error of the network. However, since the PE level is related to a specific recurrent trajectory, some of the constants in the PE level relations are trajectory-dependent, and it is difficult to give a uniform result. Fortunately, based on our observations, we can inversely derive the constant in the PE level by directly calculating the PE level from the definition of PE. Nonetheless, the precise relations of PE level still need to be confirmed by further research. In the future, the ability to improve knowledge integration of deterministic learning based on the relations of the PE level seems to be an interesting topic.

Acknowledgements This work was supported by National Natural Science Foundation of China (Grant Nos. 62350083, 62203263) and Natural Science Foundation of Shandong Province (Grant No. ZR2022QF062).

References

1 Sastry S, Bodson M. Adaptive Control: Stability, Convergence and Robustness. Upper Saddle River: Prentice Hall, 1989
2 Slotine J-J E, Li W P. Applied Nonlinear Control. Englewood Cliffs: Prentice Hall, 1991
3 Boyd S, Sastry S. On parameter convergence in adaptive control. Syst Control Lett, 1983, 3: 311–319
4 Boyd S, Sastry S S. Necessary and sufficient conditions for parameter convergence in adaptive control. Automatica, 1986, 22: 629–639
5 Narendra K S, Annaswamy A M. Persistent excitation in adaptive systems. Int J Control, 1987, 45: 127–160
6 Morgan A P, Narendra K S. On the uniform asymptotic stability of certain linear nonautonomous differential equations. SIAM J Control Optim, 1977, 15: 5–24
7 Anderson B. Exponential stability of linear equations arising in adaptive identification. IEEE Trans Automat Contr, 1977, 22: 83–88
8 Mareels I M Y, Gevers M. Persistency of excitation criteria for linear, multivariable, time-varying systems. Math Control Signal Syst, 1988, 1: 203–226
9 Songwu Lu, Basar T. Robust nonlinear system identification using neural-network models. IEEE Trans Neural Netw, 1998, 9: 407–429
10 Lin J-S, Kanellakopoulos I. Nonlinearities enhance parameter convergence in strict feedback systems. IEEE Trans Automat Contr, 1999, 44: 89–94
11 Sanner R M, Slotine J-J E. Stable recursive identification using radial basis function networks. In: Proceedings of 1992 American Control Conference, 1992. 1829–1833
12 Gorinevsky D. On the persistency of excitation in radial basis function network identification of nonlinear systems. IEEE Trans Neural Netw, 1995, 6: 1237–1244
13 Kurdila A J, Narcowich F J, Ward J D. Persistency of excitation in identification using radial basis function approximants. SIAM J Control Optim, 1995, 33: 625–642
14 Wang C, Hill D J. Learning from neural control. IEEE Trans Neural Netw, 2006, 17: 130–146
15 Park J, Sandberg I W. Universal approximation using radial-basis-function networks. Neural Comput, 1991, 3: 246–257
16 Wang M, Jiang Z, Shi H. Estimator-based dynamic learning from neural control of discrete-time strict-feedback systems. Nonlinear Dyn, 2023, 111: 21735–21746
17 Liu F, Zeng W, Yuan C, et al. Kinect-based hand gesture recognition using trajectory information, hand motion dynamics and neural networks. Artif Intell Rev, 2019, 52: 563–583
18 Jiang Y, Wang Y, Miao Z, et al. Composite-learning-based adaptive neural control for dual-arm robots with relative motion. IEEE Trans Neural Netw Learn Syst, 2022, 33: 1010–1021
19 Pan Y, Yu H. Biomimetic hybrid feedback feedforward neural-network learning control. IEEE Trans Neural Netw Learn Syst, 2017, 28: 1481–1487
20 Wang C, Hill D J. Deterministic Learning Theory for Identification, Recognition, and Control. Boca Raton: CRC Press, 2009
21 Shi H, Wang M, Wang C. Leader-follower formation learning control of discrete-time nonlinear multiagent systems. IEEE Trans Cybern, 2023, 53: 1184–1194
22 Zhao Z, He W, Zhang F, et al. Deterministic learning from adaptive neural network control for a 2-DOF helicopter system with unknown backlash and model uncertainty. IEEE Trans Ind Electron, 2023, 70: 9379–9389
23 Wu W, Hu J, Zhang F, et al. New results on rapid dynamical pattern recognition via deterministic learning from sampling sequences. IEEE Trans Neural Netw Learn Syst, 2023, 35: 12330–12343
24 Sun C, Wu W, Wang C. Time series classification of dynamical systems using deterministic learning. Nonlinear Dyn, 2023, 111: 21837–21859
25 Yuan C, Wang C. Persistency of excitation and performance of deterministic learning. Syst Control Lett, 2011, 60: 952–959
26 Wu W, Zhang J, Hu J, et al. Explicit convergence relations for a class of discrete LTV systems and its application to performance analysis of deterministic learning. J Franklin Institute, 2024, 361: 106648
27 Maghenem M A, Loría A. Strict Lyapunov functions for time-varying systems with persistency of excitation. Automatica, 2017, 78: 274–279
28 Saoud A, Maghenem M, Loría A, et al. Hybrid persistency of excitation in adaptive estimation for hybrid systems. IEEE Trans Automat Contr, 2024, 69: 8828–8835
29 Paruchuri S T, Guo J, Kurdila A. Sufficient conditions for parameter convergence over embedded manifolds using kernel techniques. IEEE Trans Automat Contr, 2023, 68: 753–765
30 Karg P, Kopf F, Braun C A, et al. Excitation for adaptive optimal control of nonlinear systems in differential games. IEEE Trans Automat Contr, 2023, 68: 596–603
31 Lekang T, Lamperski A. Sufficient conditions for persistency of excitation with step and ReLU activation functions. In: Proceedings of 2022 IEEE 61st Conference on Decision and Control (CDC), 2022. 2025–2030
32 Nar K, Sastry S. Persistency of excitation for robustness of neural networks. ArXiv:1911.01043
33 Sridhar K, Sokolsky O, Lee I, et al. Improving neural network robustness via persistency of excitation. In: Proceedings of 2022 American Control Conference (ACC), 2022. 1521–1526
34 Coulson J, Waarde H J, Lygeros J, et al. A quantitative notion of persistency of excitation and the robust fundamental lemma. IEEE Control Syst Lett, 2023, 7: 1243–1248
35 Zheng T, Wang C. Relationship between persistent excitation levels and RBF network structures, with application to performance analysis of deterministic learning. IEEE Trans Cybern, 2017, 47: 3380–3392
36 Sivakumar N, Ward J D. On the least squares fit by radial functions to multidimensional scattered data. Numer Math, 1993, 65: 219–243
37 Wu W, Wang C, Yuan C. Deterministic learning from sampling data. Neurocomputing, 2019, 358: 456–466
38 Narcowich F, Ward J, Wendland H. Sobolev bounds on functions with scattered zeros, with applications to radial basis function surface fitting. Math Comp, 2005, 74: 743–763
39 Bai E W, Sastry S S. Persistency of excitation, sufficient richness and parameter convergence in discrete time adaptive control. Syst Control Lett, 1985, 6: 153–163
40 Fradkov A L, Evans R J. Control of chaos: methods and applications in engineering. Annu Rev Control, 2005, 29: 33–56
41 Liu Q, Li D, Ge S S, et al. Adaptive feedforward RBF neural network control with the deterministic persistence of excitation. Neural Comput Appl, 2021, 33: 17013–17028
42 Zheng A, Huang Y, Na J, et al. Adaptive neural identification and non-singular control of pure-feedback nonlinear systems. ISA Trans, 2024, 144: 409–418
43 Diederichs B, Iske A. Improved estimates for condition numbers of radial basis function interpolation matrices. J Approx Theory, 2019, 238: 38–51
44 Fornberg B, Larsson E, Flyer N. Stable computations with Gaussian radial basis functions. SIAM J Sci Comput, 2011, 33: 869–892
45 Fornberg B, Wright G. Stable computation of multiquadric interpolants for all values of the shape parameter. Comput Math Appl, 2004, 48: 853–867
46 Deng M, Wang C. Gait recognition under different clothing conditions via deterministic learning. IEEE CAA J Autom Sin, 2024, 11: 1530–1532
47 Dai S L, He S, Ma Y, et al. Distributed cooperative learning control of uncertain multiagent systems with prescribed performance and preserved connectivity. IEEE Trans Neural Netw Learn Syst, 2021, 32: 3217–3229
48 Dai S L, He S, Ma Y, et al. Cooperative learning-based formation control of autonomous marine surface vessels with prescribed performance. IEEE Trans Syst Man Cybern Syst, 2022, 52: 2565–2577
49 Wang B. Distributed error estimation for quasi-synchronization of heterogeneous dynamical networks. IEEE Trans Automat Contr, 2022, 67: 2489–2496
50 Wang B. A distributed adaptive observer-based approach to synchronization of heterogeneous nonmonotonic nonlinear systems for formation application. IEEE Trans Automat Contr, 2024, 69: 6137–6152
51 Rössler O E. An equation for continuous chaos. Phys Lett A, 1976, 57: 397–398
52 Chen G R, Dong X N. From Chaos to Order: Methodologies, Perspectives and Applications. Singapore: World Scientific, 1998
53 Narcowich F J, Ward J D. Norms of inverses and condition numbers for matrices associated with scattered data. J Approx Theory, 1991, 64: 69–94

Appendix A Rewriting and extending the proof of Proposition 3.12 in [36]

Proof. From (37) and the proof of Proposition 3.12 in [36] (the incorrect factor π^n is omitted), we see that

$$\begin{aligned} J_\zeta &= \frac{\eta^n}{(2\pi)^n}\int_{\mathbb{R}^n} \mathrm{e}^{-\frac{\|u\|^2\eta^2}{4}}\left[\sum_{j,l=1}^{N_\zeta} c_j c_l \mathrm{e}^{-\mathrm{i}(\xi_j-\xi_l)u}\left(1-\mathrm{e}^{-\mathrm{i}d_j u}\right)\right]\mathrm{d}u \\ &= \sum_{j,l=1}^{N_\zeta} c_j c_l \frac{\eta^n}{(2\pi)^n}\int_{\mathbb{R}^n}\left(1-\mathrm{e}^{-\mathrm{i}d_j u}\right)\mathrm{e}^{-\frac{\|u\|^2\eta^2}{4}}\mathrm{e}^{\mathrm{i}(\xi_l-\xi_j)u}\mathrm{d}u \\ &= \sum_{j,l=1}^{N_\zeta} c_j c_l \frac{1}{(2\pi)^n}\int_{\mathbb{R}^n}\left(1-\mathrm{e}^{-\mathrm{i}d_j u}\right)\widehat{F}(u)\,\mathrm{e}^{\mathrm{i}(\xi_l-\xi_j)u}\mathrm{d}u, \end{aligned} \tag{72}$$

where $d_j := Z_j - \xi_j$, $c = \left[c_1, \ldots, c_{N_\zeta}\right]^{\mathrm{T}} \in \mathbb{R}^{N_\zeta}$ is an arbitrary unit constant vector with c_j, c_l are its components, $\widehat{F}(u)$ denotes the generalized Fourier transform function of $\mathrm{e}^{-\frac{\|x\|^2}{\eta^2}}$.

By setting $\nabla_{d_j} g(\cdot) := g(\cdot) - g(\cdot - d_j)$, $g : \mathbb{R}^n \to \mathbb{R}$, (72) can be rewritten as follows:

$$\begin{aligned} J_\zeta &= \sum_{j,l=1}^{N_\zeta} c_j c_l \frac{1}{(2\pi)^n}\int_{\mathbb{R}^n}\left(\nabla_{d_j}F\right)^{\wedge}(u)\,\mathrm{e}^{\mathrm{i}(\xi_l-\xi_j)u}\mathrm{d}u \\ &= \sum_{j,l=1}^{N_\zeta} c_j c_l \left(\nabla_{d_j}F\right)(\xi_l-\xi_j) \\ &= \sum_{j=1}^{N_\zeta} |c_j|^2\left(\nabla_{d_j}F\right)(0) + \sum_{j,l=1,j\neq l}^{N_\zeta} c_j c_l\left(\nabla_{d_j}F\right)(\xi_l-\xi_j). \end{aligned} \tag{73}$$

Further scaling can be achieved by taking the absolute value on both sides.

$$\begin{aligned} |J_\zeta| &\leqslant \sum_{j=1}^{N_\zeta} |c_j|^2\left|\left(\nabla_{d_j}F\right)(0)\right| + {\sum_{j,l=1}^{N_\zeta}}' |c_j c_l|\left|\left(\nabla_{d_j}F\right)(\xi_l-\xi_j)\right| \\ &=: \mathbb{S}_1 + \mathbb{S}_2, \end{aligned} \tag{74}$$

where $\sum'$ in (74) indicates that $j \neq l$ in that sum.

We first estimate $\mathbb{S}_1$ by applying the following scaling:

$$\left|\left(\nabla_{d_j}F\right)(0)\right| = \left|1-\mathrm{e}^{-\frac{\|d_j\|^2}{\eta^2}}\right| \leqslant \frac{\|d_j\|^2}{\eta^2} \leqslant \frac{\varepsilon^2}{\eta^2} \tag{75}$$

for each $1 \leqslant j \leqslant N_\zeta$. Then, we have

$$\mathbb{S}_1 \leqslant \frac{\varepsilon^2}{\eta^2}\|c\|^2. \tag{76}$$

We next estimate $\mathbb{S}_2$, first applying the following scaling:

$$\begin{aligned} \mathbb{S}_2 &\leqslant {\sum_{j,l=1}^{N_\zeta}}' |c_j c_l|\left|\left(\nabla_{d_j}F\right)(\xi_l-\xi_j)\right| \\ &\leqslant {\sum_{j,l=1}^{N_\zeta}}' \frac{|c_j|^2+|c_l|^2}{2}\left|\left(\nabla_{d_j}F\right)(\xi_l-\xi_j)\right| \\ &\leqslant \max\left\{\Upsilon_{N_\zeta}, \widetilde{\Upsilon}_{N_\zeta}\right\}\|c\|^2, \end{aligned} \tag{77}$$

where

$$\begin{aligned}\Upsilon_{N_\zeta} &:= \max_j \sum_{l=1}^{N_\zeta}{}' \left|\left(\nabla_{d_j} F\right)(\xi_l-\xi_j)\right|,\\ \widetilde{\Upsilon}_{N_\zeta} &:= \max_l \sum_{j=1}^{N_\zeta}{}' \left|\left(\nabla_{d_j} F\right)(\xi_l-\xi_j)\right|.\end{aligned}\tag{78}$$

Let j_0 and l_0 be the indices where the maximum values of Υ_{N_ζ} and $\widetilde{\Upsilon}_{N_\zeta}$ are attained, respectively. In our further estimation of Υ_{N_ζ}, we first suppose that $y \in \mathbb{R}^n$ with $\|y\| \geqslant h$ and $0 < \|d_j\| \leqslant \varepsilon \leqslant 2h$. Then, by applying the mean value theorem, we have the following for $1 \leqslant j \leqslant N_\zeta$:

$$\begin{aligned}\left|\left(\nabla_{d_j} F\right)(y)\right| &= \left|\mathrm{e}^{-\frac{\|y\|^2}{\eta^2}} - \mathrm{e}^{-\frac{\|y-d_j\|^2}{\eta^2}}\right|\\ &\leqslant \frac{2\|d_j\|}{\eta^2}\left[\|y\|+\|d_j\|\right]\mathrm{e}^{-\frac{\left[\min\{\|y\|,\|y-d_j\|\}\right]^2}{\eta^2}}\\ &\leqslant \frac{2\varepsilon}{\eta^2}\left[\|y\|+\varepsilon\right]\mathrm{e}^{-\frac{\left[\min\{\|y\|,\|y-d_j\|\}\right]^2}{\eta^2}}\\ &\leqslant \frac{2\varepsilon}{\eta^2}\left[\|y\|+\varepsilon\right]\mathrm{e}^{-\frac{\left[\|y\|-\|d_j\|\right]^2}{\eta^2}}\\ &\leqslant \frac{2\varepsilon}{\eta^2}\left[\|y\|+\varepsilon\right]\mathrm{e}^{-\frac{\left[\|y\|-\varepsilon\right]^2}{\eta^2}}.\end{aligned}\tag{79}$$

Therefore,

$$\begin{aligned}\Upsilon_{N_\zeta} &= \sum_{l=1}^{N_\zeta}{}' \left|\left(\nabla_{d_j} F\right)(\xi_l-\xi_{j_0})\right|\\ &\leqslant \frac{2\varepsilon}{\eta^2}\sum_{l=1}^{N_\zeta}{}' \left[\|\xi_l-\xi_{j_0}\|+\varepsilon\right]\mathrm{e}^{-\frac{\left[\|\xi_l-\xi_{j_0}\|-\varepsilon\right]^2}{\eta^2}}.\end{aligned}\tag{80}$$

By following [53], we conclude from the above that

$$\Upsilon_{N_\zeta} \leqslant \frac{6n\varepsilon}{\eta^2}\sum_{i=1}^{\infty}(i+2)^{n-1}\,\mathbb{K}_i,\tag{81}$$

where

$$\begin{aligned}\mathbb{K}_i &:= \sup\left\{\left[\|\xi\|+\varepsilon\right]\mathrm{e}^{-\frac{\left[\|x\|-\varepsilon\right]^2}{\eta^2}};\, ih < \|\xi\| \leqslant (i+1)\,h\right\}\\ &\leqslant \left[(i+1)\,h+\varepsilon\right]\mathrm{e}^{-\frac{\left[ih-\varepsilon\right]^2}{\eta^2}}.\end{aligned}\tag{82}$$

Since $\varepsilon \leqslant 2h$,

$$\Upsilon_{N_\zeta} \leqslant \frac{6nh\varepsilon}{\eta^2}\sum_{i=1}^{\infty}(i+2)^{n-1}(i+3)\,\mathrm{e}^{-\frac{(i-2)^2h^2}{\eta^2}}.\tag{83}$$

The same argument also demonstrates that

$$\widetilde{\Upsilon}_{N_\zeta} \leqslant \frac{6nh\varepsilon}{\eta^2}\sum_{i=1}^{\infty}(i+2)^{n-1}(i+3)\,\mathrm{e}^{-\frac{(i-2)^2h^2}{\eta^2}}.\tag{84}$$

Combining (74), (76), (77) and taking $\|c\| = 1$ yields

$$|J_\zeta| \leqslant \frac{\varepsilon^2}{\eta^2} + \frac{6nh\varepsilon}{\eta^2}\sum_{i=1}^{\infty}(i+2)^{n-1}(i+3)\,\mathrm{e}^{-\frac{(i-2)^2h^2}{\eta^2}}.\tag{85}$$

On the other hand, we suppose that $2h < \|d_j\| \leqslant \varepsilon \leqslant \varepsilon'$. Then, (79) be rewritten as

$$\left|\left(\nabla_{d_j} F\right)(y)\right| \leqslant \frac{2\varepsilon}{\eta^2}\left[\|y\|+\varepsilon\right] \mathrm{e}^{-\frac{\left[\min\left\{\|y\|,\left\|y-d_j\right\|\right\}\right]^2}{\eta^2}}. \tag{86}$$

Therefore,

$$\begin{aligned}\Upsilon_{N_\zeta} &= {\sum_{l=1}^{N_\zeta}}{}' \left|\left(\nabla_{d_j} F\right)\left(\xi_l-\xi_{j_0}\right)\right| \\ &\leqslant \frac{2\varepsilon}{\eta^2} {\sum_{l=1}^{N_\zeta}}{}' \left[\left\|\xi_l-\xi_{j_0}\right\|+\varepsilon\right] \mathrm{e}^{-\frac{\left[\min\left\{\left\|\xi_l-\xi_{j_0}\right\|,\left\|\xi_l-\xi_{j_0}-d_j\right\|\right\}\right]^2}{\eta^2}}.\end{aligned} \tag{87}$$

Then, by following [53], we again further deduce that

$$\Upsilon_{N_\zeta} \leqslant \frac{6n\varepsilon}{\eta^2} \sum_{i=1}^{\infty} (i+2)^{n-1} \mathbb{K}_i, \tag{88}$$

where

$$\begin{aligned}\mathbb{K}_i &:= \sup\left\{\left[\|\xi\|+\varepsilon\right] \mathrm{e}^{-\frac{\left[\min\left\{\|\xi\|,\left\|\xi-d_j\right\|\right\}\right]^2}{\eta^2}}; ih < \|\xi\| \leqslant (i+1)h\right\} \\ &\leqslant \begin{cases}\left[(i+1)h+\varepsilon\right] \mathrm{e}^{-\frac{i^2h^2}{\eta^2}}, \ \|\xi\| \leqslant \dfrac{\|d_j\|}{2}, \\ \left[(i+1)h+\varepsilon\right] \mathrm{e}^{-\frac{(ih-\varepsilon)^2}{\eta^2}}, \ \|\xi\| > \dfrac{\|d_j\|}{2}.\end{cases}\end{aligned} \tag{89}$$

Since $\varepsilon \leqslant \varepsilon'$,

$$\begin{aligned}\Upsilon_{N_\zeta} &\leqslant \frac{6n\varepsilon}{\eta^2} \sum_{i=1}^{\left\lfloor \frac{\|d_j\|}{2h} \right\rfloor} (i+2)^{n-1}\left[(i+1)h+\varepsilon\right] \mathrm{e}^{-\frac{i^2h^2}{\eta^2}} + \frac{6n\varepsilon}{\eta^2} \sum_{i=\left\lceil \frac{\|d_j\|}{2h} \right\rceil}^{\infty} (i+2)^{n-1}\left[(i+1)h+\varepsilon\right] \mathrm{e}^{-\frac{(ih-\varepsilon)^2}{\eta^2}} \\ &\leqslant \frac{6nh\varepsilon}{\eta^2} \sum_{i=1}^{\left\lfloor \frac{\varepsilon}{2h} \right\rfloor} (i+2)^{n-1}\left[i+1+\frac{\varepsilon}{h}\right] \mathrm{e}^{-\frac{i^2h^2}{\eta^2}} + \frac{6nh\varepsilon}{\eta^2} \sum_{i=1}^{\infty} (i+2)^{n-1}\left[i+1+\frac{\varepsilon}{h}\right] \mathrm{e}^{-\frac{\left(i-\frac{\varepsilon}{h}\right)^2h^2}{\eta^2}}.\end{aligned} \tag{90}$$

Again combining (74), (76), (77) and taking $\|c\|=1$ yields

$$|J_\zeta| \leqslant \frac{\varepsilon^2}{\eta^2} + \frac{6nh\varepsilon}{\eta^2} \sum_{i=1}^{\left\lfloor \frac{\varepsilon}{2h} \right\rfloor} (i+2)^{n-1}\left[i+1+\frac{\varepsilon}{h}\right] e^{-\frac{i^2h^2}{\eta^2}} + \frac{6nh\varepsilon}{\eta^2} \sum_{i=1}^{\infty} (i+2)^{n-1}\left[i+1+\frac{\varepsilon}{h}\right] e^{-\frac{\left(i-\frac{\varepsilon}{h}\right)^2h^2}{\eta^2}}. \tag{91}$$

Finally, we set $k_\eta = \frac{\eta}{h}$ and $k_\varepsilon = \frac{\varepsilon}{h}$ and combine (85) and (91) together to obtain the following:

$$|J_\zeta| \leqslant \begin{cases}\dfrac{k_\varepsilon^2}{k_\eta^2} + 6n\dfrac{k_\varepsilon}{k_\eta^2} f_1\left(\dfrac{1}{k_\eta^2}\right), \ 0 < k_\varepsilon \leqslant 2, \\ \dfrac{k_\varepsilon^2}{k_\eta^2} + 6n\dfrac{k_\varepsilon}{k_\eta^2} f_2\left(\dfrac{1}{k_\eta^2}\right), \ 2 < k_\varepsilon \leqslant k_{\varepsilon'},\end{cases} \tag{92}$$

where $f_1(x) = \sum_{i=1}^{\infty} (i+2)^{n-1}(i+3)\mathrm{e}^{-(i-2)^2x}$ and $f_2(x) = \sum_{i=1}^{\left\lfloor \frac{k_\varepsilon}{2} \right\rfloor} (i+2)^{n-1}(i+1+k_\varepsilon)\mathrm{e}^{-i^2x} + \sum_{i=1}^{\infty}(i+2)^{n-1} \times (i+1+k_\varepsilon)\mathrm{e}^{-(i-k_\varepsilon)^2x}$.